Supporting Information for

AIE-active metal-organic frameworks: facile preparation, tunable light emission,

**ultrasensitive sensing of copper (II) and visual fluorescence detection of glucose**

Siqi Xie[1], Qi Liu*[,1], Fawei Zhu[1], Miao Chen[1,2], Lumin Wang[1], Yu Xiong[3], Yuqiu Zhu[1], Yu

Zheng[1], Xiaoqing Chen*[,1]

[1]*College of Chemistry and Chemical Engineering, Key Laboratory of Hunan Province for*

Water Environment and Agriculture Product Safety, Central South University, Changsha

410083, Hunan, China.

[2]*School of Life Sciences, Central South University, Changsha 410083, Hunan, China.*

[3]*Department of Chemistry, Tsinghua University, Beijing 100084, China*

E-mail address: iliuqi@csu.edu.cn (Qi Liu), xqchen@csu.edu.cn (Xiaoqing Chen)
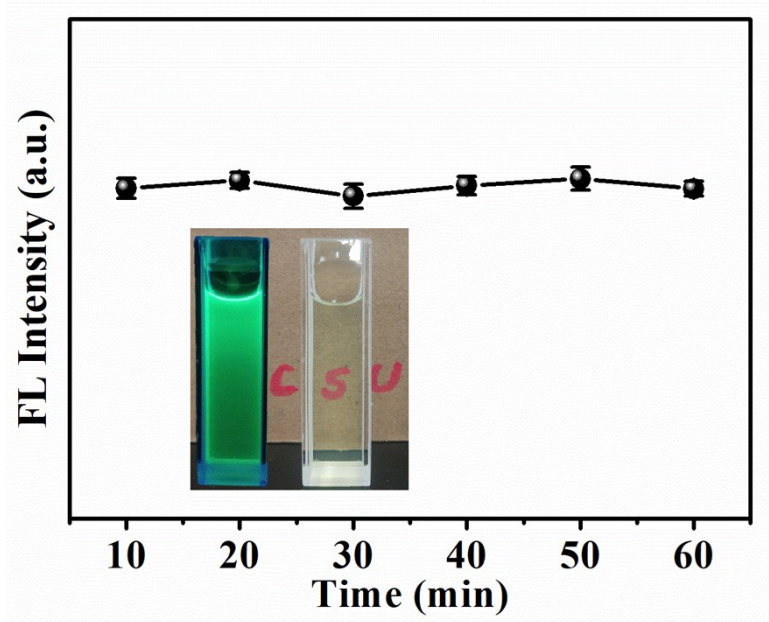
Figure S1 AIE-active MOFs solution was placed under the UV lamp of 365 nm for continuous

irradiation for one hour in the static conditions, and the fluorescence intensity was measured every

10 mins at the excitation wavelength of 365 nm, indicating the resulted LOMF possesses good
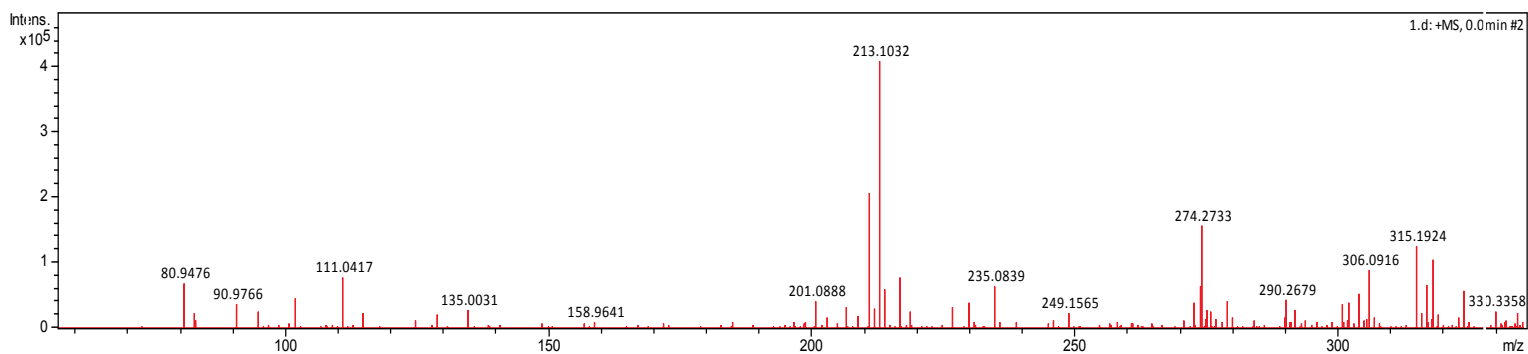
dispersibility. Insert view: LMOF-2 solution under 365 nm UV lamp (right), and high

transparence of LMOF-2 solution (left), the background is a cardboard.

$R_2 = Cl$ $R_4 = F, Cl, Br, CH_3, OCH_3, N(CH_2CH_3)_2$
$R_3 = F, Cl, Br$ $R_5 = F, Cl, Br$
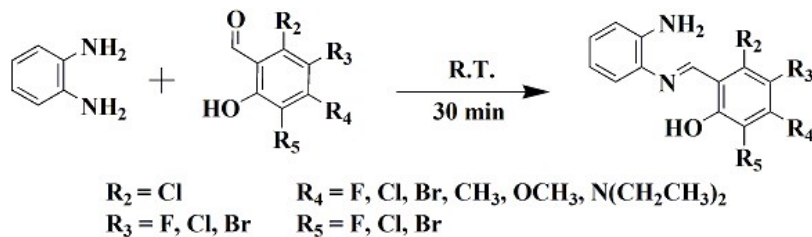
Figure S2 Synthetic routes of APMP and its derivatives.
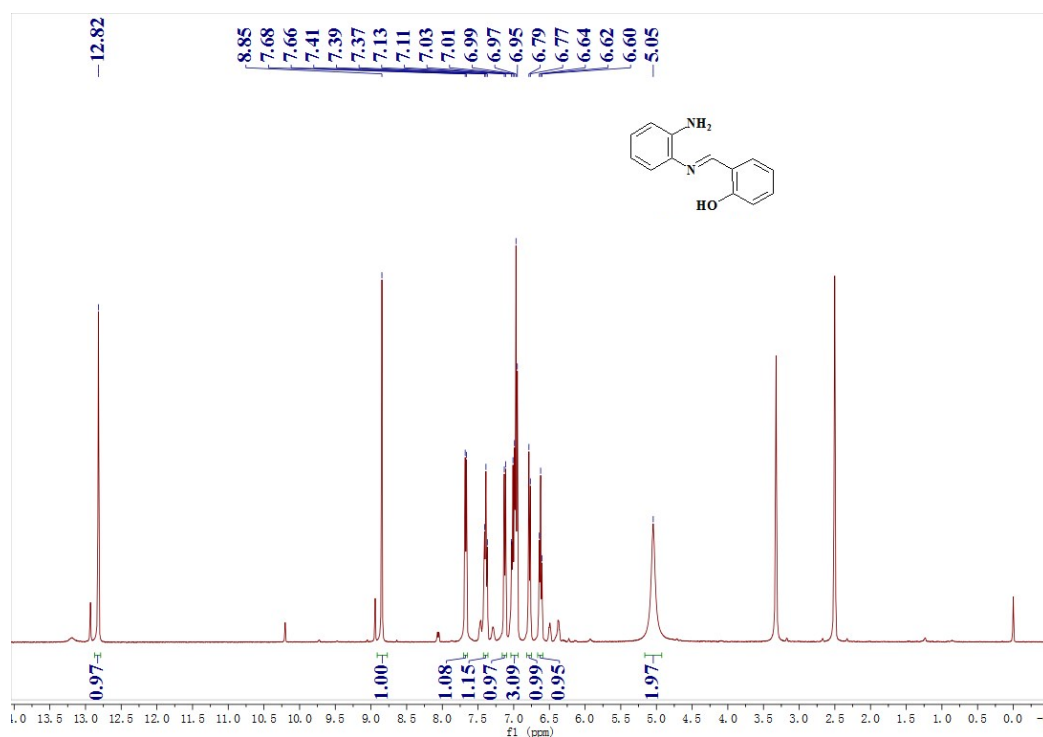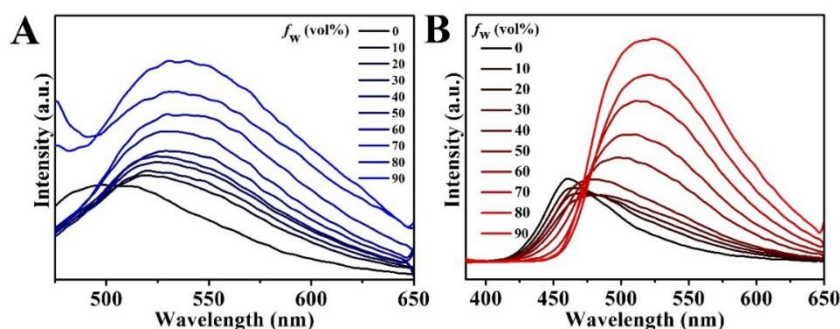

Figure S3 ^{1}H NMR spectrum of APMP in DMSO-d6.


Figure S4 High-resolution mass spectra (HRMS) of APMP.

Characterization date of APMP, yellow solid, 82% yield, ^{1}H NMR (DMSO-*d6*, 400 MHz)

δ 12.82 (s, 1H), 8.85 (s, 1H), 7.67 (d, *J* = 7.2 Hz, 1H), 7.39 (t, *J* = 7.6 Hz, 1H), 7.12 (d, *J* = 7.6

Hz, 1H), 7.03-6.95 (m, 3H), 6.78 (d, *J* = 7.2 Hz, 1H), 6.23 (t, *J* = 7.6 Hz, 1H), 5.05 (s, 1H);

2

HRMSEI(+) calcd for $C_{13}H_{13}N_2O^+$ [M+1]$^+$ 213.1022, found 213.1032;

Figure S5 The typical AIE phenomenon of APMP (A) and APMP-2 (B).

1. Thermal gravimetric analysis (TGA)
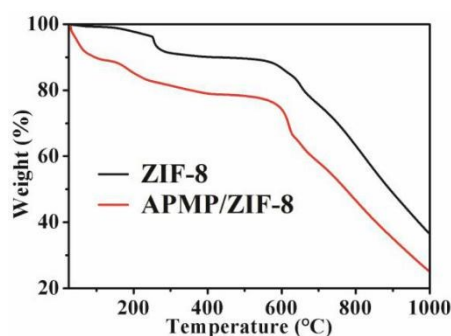
Figure S6 TGA of ZIF-8 and APMP/ZIF-8.

The first-stage decomposition of the APMP/ZIF-8 composite started from 30°C and plateaued around 500°C with about 20% weight loss due to the remove of residual solvent and the decomposition of APMP, which is slightly higher than that the pure ZIF-8 crystal (400°C) resulted from the presence of APMP conjugated on the surface of ZIF-8. After 500°C, the weight loss can be attributed to the decomposition of framework. During 500-700°C, only about 20% weight loss reflects the good thermal stability of ZIF-8 and APMP/ZIF-8. And the functionalization ratio of APMP on the APMP/ZIF-8 was calculated to be about 12.66 %.

2. ^{1}H, ^{13}C NMR spectra and HRMS of APMP derivatives

Characterization date of APMP-1: yellow solid, 63% yield, ^{1}H NMR (DMSO-*d6*, 400 MHz) δ 13.46 (s, 1H), 8.85 (s, 1H), 7.74 (t, *J* = 7.6 Hz, 1H), 7.12 (d, *J* = 0.8 Hz, 1H), 7.03-6.99 (m, 1H), 6.84-6.77 (m, 3H), 6.64-6.60 (m, 1H), 5.06 (s, 2H); 13C NMR (DMSO-*d6*, 100 MHz,) δ 165.11, 163.41, 162.62, 160.46, 143.05, 134.60, 134.34, 128.28, 118.89, 117.62, 117.17 , 115.85 , 107.06, 103.85; HRMSEI(+) calcd for $C_{13}H_{12}FN_2O^+$ [M+1]$^+$ 231.0928, found 231.0926;

Characterization date of APMP-2 yellow solid, 83% yield, ^{1}H NMR (DMSO-*d6*, 400 MHz) δ

13.18 (s, 1H), 8.86 (s, 1H), 7.72 (d, J = 7.6 Hz, 1H), 7.13 (d, J = 8.0 Hz, 1H), 7.04-7.00 (m, 3H), 6.78 (d, J = 8.0 Hz, 1H), 6.62 (t, J = 7.2 Hz, 1H), 5.10 (s, 2H); 13C NMR (DMSO-$d6$, 100 MHz) δ 161.2, 159.7, 143.3, 137.2, 134.3, 133.458, 128.48, 119.74, 119.63, 118.78, 117.14, 116.76, 115.89; HRMSEI(+) calcd for $C_{13}H_{12}ClN_2O^+$ [M+1]$^+$ 247.0633, found 247.0631;

Characterization date of APMP-3: yellow solid, 88% yield, ^{1}H NMR (DMSO-$d6$, 400 MHz) δ 13.12 (s, 1H), 8.85 (s, 1H), 7.65 (d, J = 8.0 Hz, 1H), 7.19-7.12 (m, 3H), 7.04-7.00 (m, 1H), 6.78 (dd, J = 8.0, 1.2 Hz, 1H), 6.64-6.60 (m, 1H), 5.10 (s, 2H); 13C NMR (DMSO-$d6$, 100 MHz) δ 161.06, 159.77, 143.3, 134.33, 133.64, 128.50, 126.05, 122.61, 119.94, 119.72, 118.75, 117.17, 115.92; HRMSEI(+) calcd for $C_{13}H_{12}BrN_2O^+$ [M+1]$^+$ 291.0128, found 291.0111;

Characterization date of APMP-4: yellow solid, 90% yield, ^{1}H NMR (DMSO-d6, 400 MHz) δ 12.78 (s, 1H), 8.88 (s, 1H), 7.48-7.44 (m, 2H), 7.14 (dd, J = 8.0, 1.2 Hz, 1H), 7.06-7.02 (m, 1H), 6.79 (dd, J = 8.0, 0.8 Hz, 1H), 6.64-6.61 (m, 1H), 5.20 (s, 2H); 13C NMR (DMSO-$d6$, 100 MHz) δ 158.53 , 154.01, 150.82, 144.94, 143.65, 133.86, 128.96, 122.38, 118.72, 117.06, 116.03, 112.25, 107.85; HRMSEI(+) calcd for $C_{13}H_{11}F_2N_2O^+$ [M+1]$^+$ 249.0834, found 249.0807;

Characterization date of APMP-5: red solid, 94% yield, ^{1}H NMR (DMSO-$d6$, 400 MHz) δ 14.28 (s, 1H), 8.90 (s, 1H), 7.75-7.71 (m, 2H), 7.17 (dd, J = 8.0, 0.8 Hz, 1H), 7.08-7.04 (m, 1H), 6.81 (dd, J = 7.6, 0.8 Hz, 1H), 6.67-6.63 (m, 1H), 5.26 (s, 2H); 13C NMR (DMSO-$d6$, 100 MHz) δ 159.96, 155.83, 143.42, 132.95, 132.02, 130.64, 129.18, 122.46, 121.91, 121.76, 119.18, 117.24, 116.35; HRMSEI(+) calcd for $C_{13}H_{11}Cl_2N_2O^+$ [M+1]$^+$ 281.0243, found 281.0226;

Characterization date of APMP-6: orange solid, 96% yield, ^{1}H NMR (DMSO-$d6$, 400 MHz) δ 14.42 (s, 1H), 8.87 (s, 1H), 7.90-7.89 (m, 2H), 7.18 (dd, J = 8.0, 0.8 Hz, 1H), 7.08-7.04 (m, 1H), 6.81 (dd, J = 8.0, 0.8 Hz, 1H), 6.67-6.63 (m, 1H), 5.21 (s, 2H); 13C NMR (DMSO-$d6$, 100 MHz) δ 159.98, 157.26, 143.41, 137.29, 134.28，132.82，129.18, 122.14, 119.25, 117.27, 116.38, 111.77, 109.83; HRMSEI(+) calcd for $C_{13}H_{11}Br_2N_2O^+$ [M+1]$^+$ 368.9233, found 368.9219;
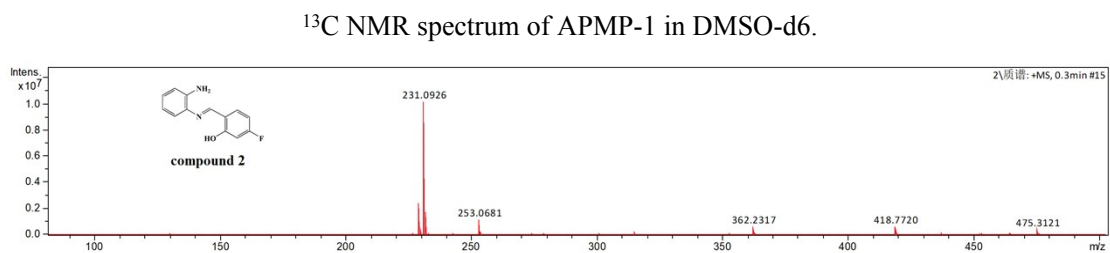
Characterization date of APMP-7: yellow solid, 66% yield, ^{1}H NMR (DMSO-$d6$, 400 MHz) δ 12.83 (s, 1H), 8.79 (s, 1H), 7.53 (d, J = 8.4 Hz, 1H), 7.11 (dd, J = 7.6, 0.8 Hz, 1H), 7.02-6.97 (m, 1H), 6.80-6.76 (m, 3H), 6.64-6.60 (m, 1H), 5.02 (s, 2H), 2.32 (s, 3H); 13C NMR (DMSO-$d6$, 100 MHz) δ 161.19, 160.36, 143.79, 142.99, 134.77, 132.46, 128.04, 120.62, 118.73, 118.05, 117.19, 117.16, 115.74, 21.88; HRMSEI(+) calcd for $C_{14}H_{15}N_2O^+$ [M+1]$^+$ 227.1179, found 227.1181;
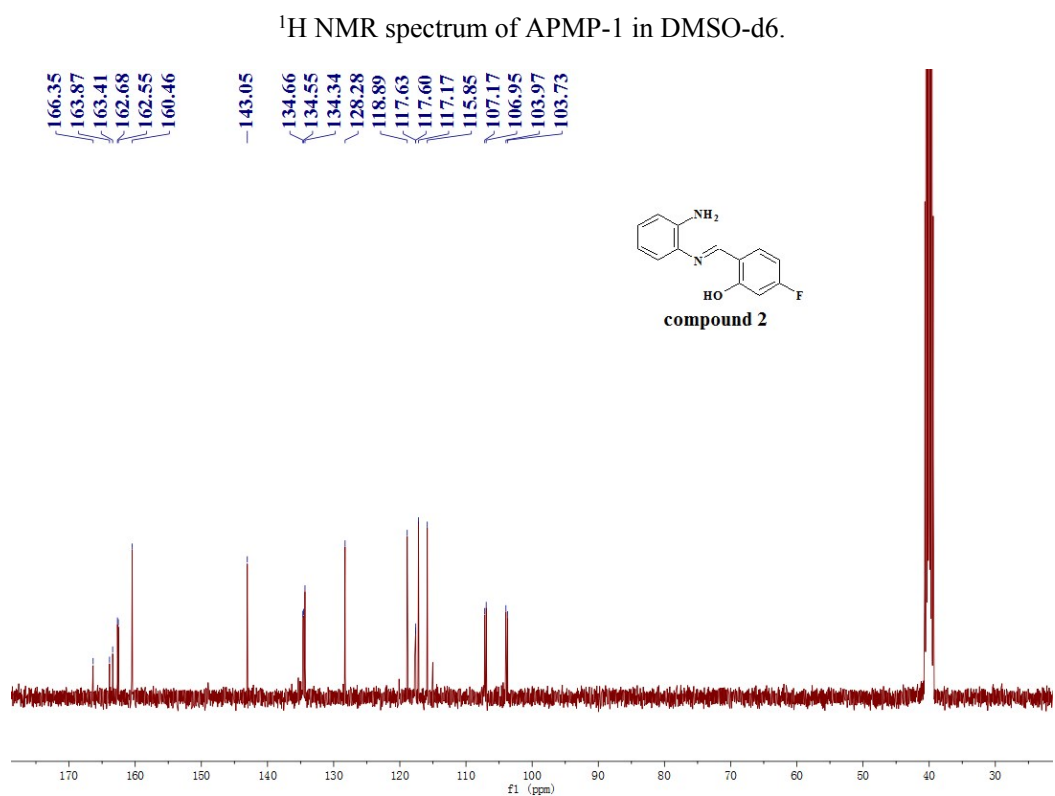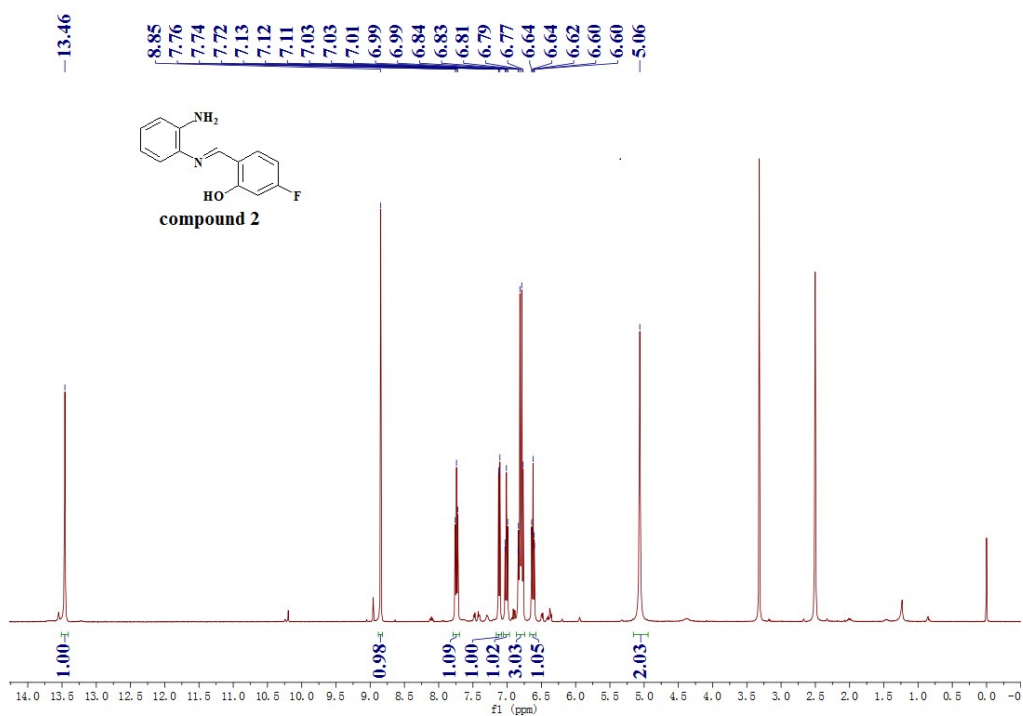
Characterization date of APMP-8: yellow solid, 76% yield, ^{1}H NMR (DMSO-$d6$, 400 MHz) δ
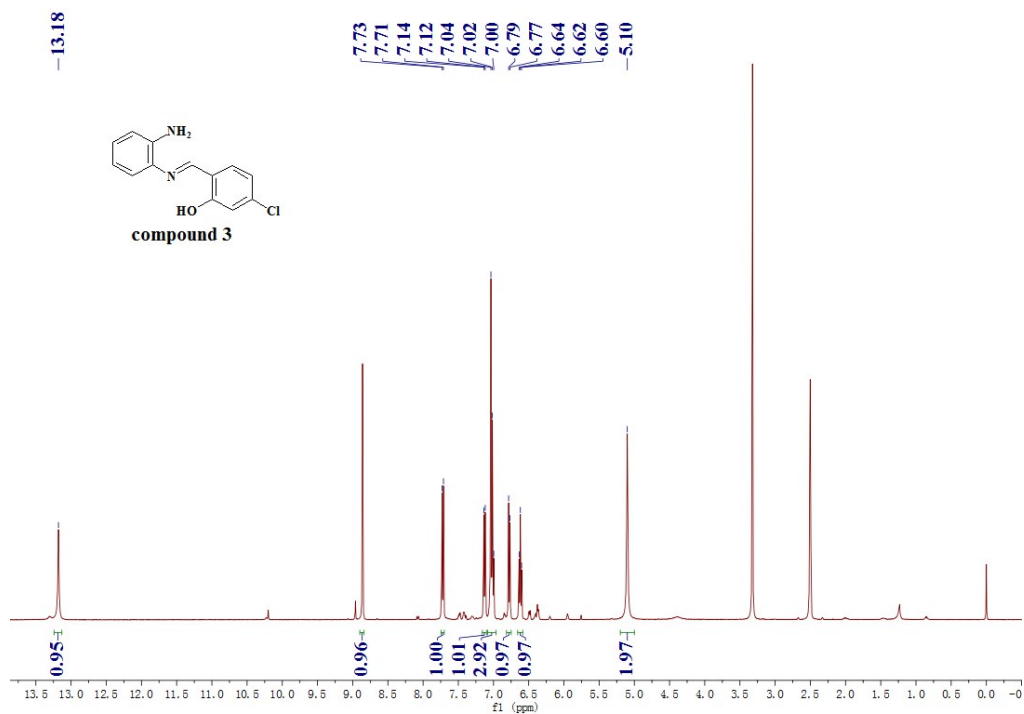
13.36 (s, 1H), 8.75 (s, 1H), 7.55 (d, J = 8.4 Hz, 1H), 7.09 (dd, J = 8.0, 1.2 Hz, 1H), 7.00-6.96 (m, 1H), 6.77 (dd, J = 8.0, 1.2 Hz, 1H), 6.64-6.59 (m, 1H), 6.56 (dd, J = 8.5, 1.2 Hz, 1H), 6.50 (d, J = 2.0 Hz, 1H), 4.98 (s, 2H), 3.81 (s, 3H); 13C NMR (DMSO-$d6$, 100 MHz) δ 163.68, 162.88, 161.07, 142.74, 134.73, 134.11, 127.73, 118.75, 117.25, 115.71, 114.08, 106.98, 101.24, 56.51, 55.89, 19.02; HRMSEI(+) calcd for $C_{14}H_{15}N_2O_2^+$ [M+1]$^+$ 243.1128, found 243.1147;

Characterization date of APMP-9: yellow solid, 73% yield, ^{1}H NMR (DMSO-$d6$, 400 MHz) δ 13.29 (s, 1H), 8.56 (s, 1H), 7.33 (d, J = 8.8 Hz, 1H), 7.03 (dd, J = 8.0, 1.2 Hz, 1H), 6.95-6.91 (m, 1H), 6.75 (dd, J = 8.0, 1.2 Hz, 1H), 6.62-6.58 (m, 1H), 6.30 (dd, J = 8.4, 2.4 Hz, 1H), 6.09 (d, J = 2.4 Hz, 1H), 4.86 (s, 2H), 3.39 (q, J = 2.8 Hz, 4H), 1.12 (t, J = 6.8 Hz, 6H); 13C NMR (DMSO-$d6$, 100 MHz) δ 163.02, 160.68, 151.62, 142.36, 135.42, 134.26, 126.82, 118.36, 117.32, 115.44, 109.53, 97.35, 44.39, 13.02; HRMSEI(+) calcd for $C_{17}H_{22}N_3O^+$ [M+1]$^+$ 284.1757, found 284.1767;
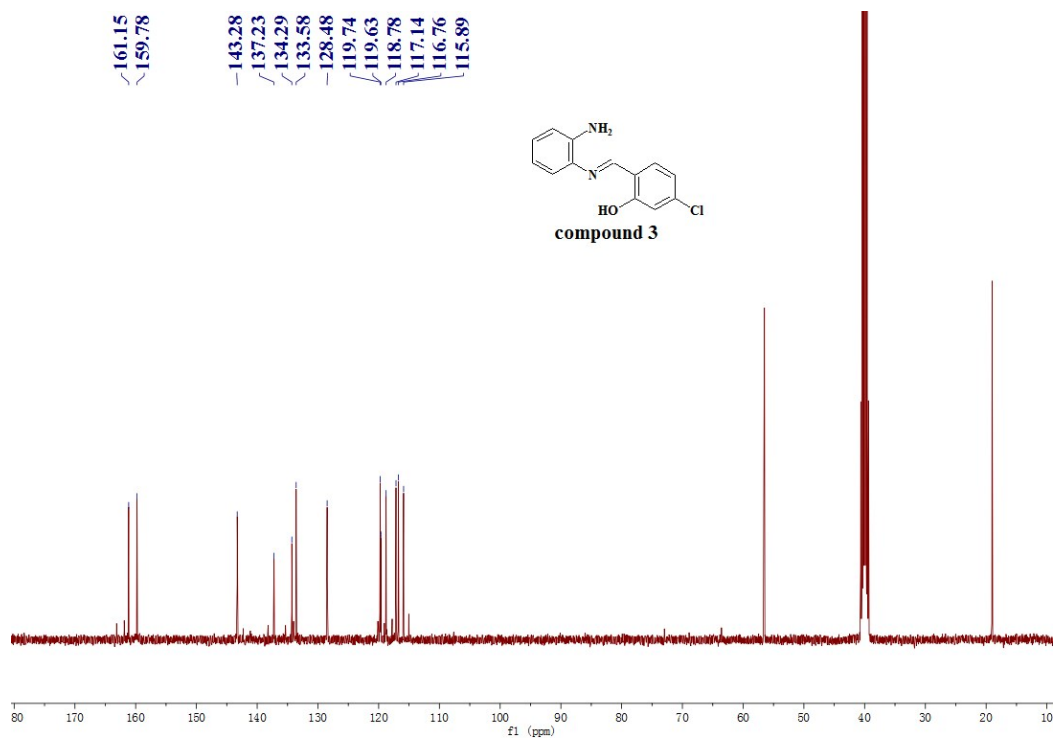
Characterization date of APMP-10: yellow solid, 83% yield, ^{1}H NMR (DMSO-$d6$, 400 MHz) δ 14.21 (s, 1H), 9.05 (s, 1H), 7.40 (t, J = 7.40, 1H), 7.16 (dd, J = 8.0, 1.2 Hz, 1H), 7.08-7.04 (m, 2H), 6.97 (d, J = 8.4 Hz, 1H), 6.82 (dd, J = 8.0, 0.8 Hz, 1H), 6.67-6.63 (m, 1H), 5.17 (s, 2H); 13C NMR (DMSO-$d6$, 100 MHz) δ 162.58, 158.03, 143.18, 135.37, 134.17, 133.93, 128.98, 120.42, 119.28, 117.39, 116.84, 116.55, 116.10; HRMSEI(+) calcd for $C_{13}H_{12}ClN_2O^+$ [M+1]$^+$ 247.0633, found 247.0604;

Characterization date of APMP-11: yellow solid, 89% yield, ^{1}H NMR (DMSO-$d6$, 400 MHz) δ 12.63 (s, 1H), 8.83 (s, 1H), 7.80 (s, 1H), 7.40 (d, J = 8.0 Hz, 1H), 7.11-6.98 (m, 3H), 6.78 (d, J = 7.)2 Hz, 1H), 6.64-6.60 (m, 1H), 5.12 (s, 2H); 13C NMR (DMSO-$d6$, 100 MHz) δ 158.86, 143.46, 134.44, 132.54, 130.74, 128.58, 123.04, 118.9, 117.1, 115.9; HRMSEI(+) calcd for $C_{13}H_{12}ClN_2O^+$ [M+1]$^+$ 247.0633, found 247.0621;

^{1}H NMR spectrum of APMP-1 in DMSO-d6.

^{13}C NMR spectrum of APMP-1 in DMSO-d6.

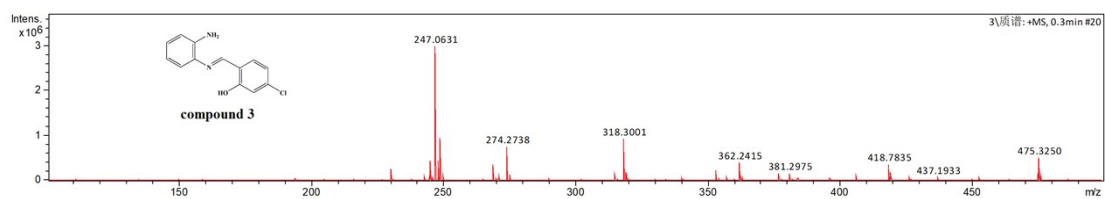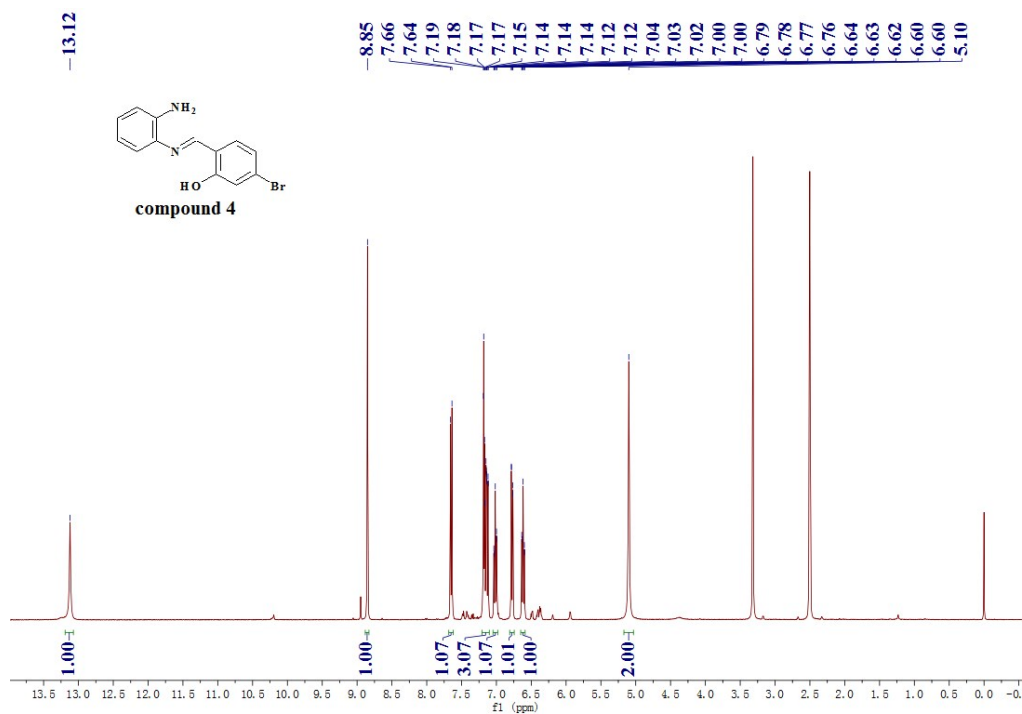High-resolution mass spectra (HRMS) of APMP-1.

^{1}H NMR spectrum of APMP-2 in DMSO-d6.

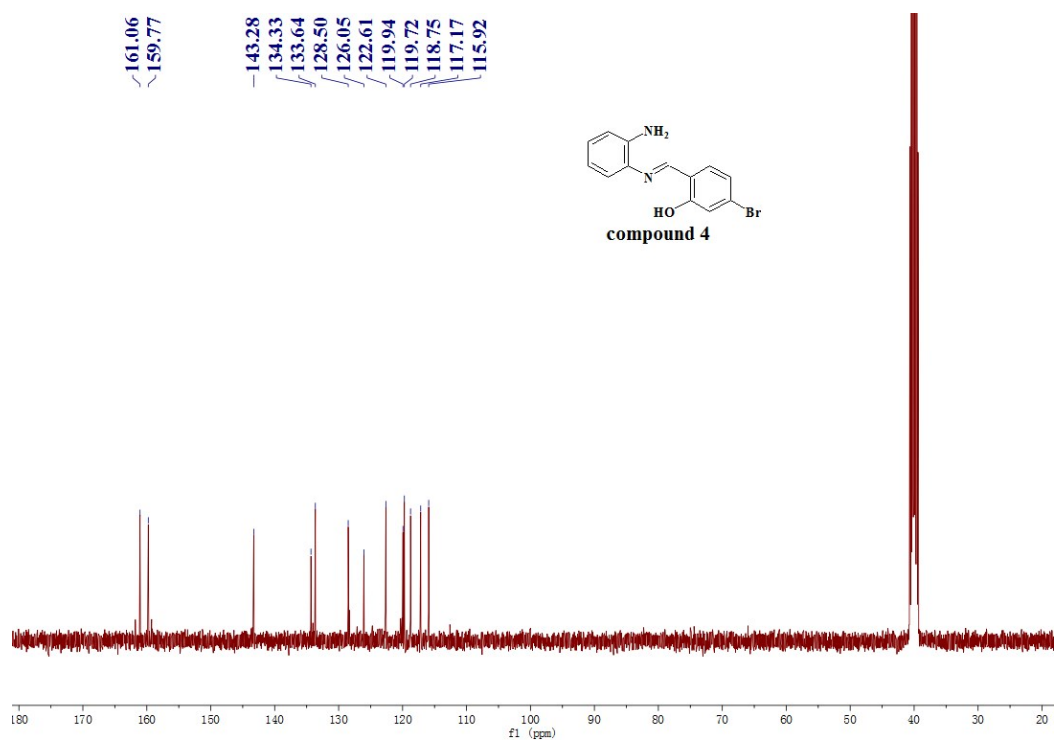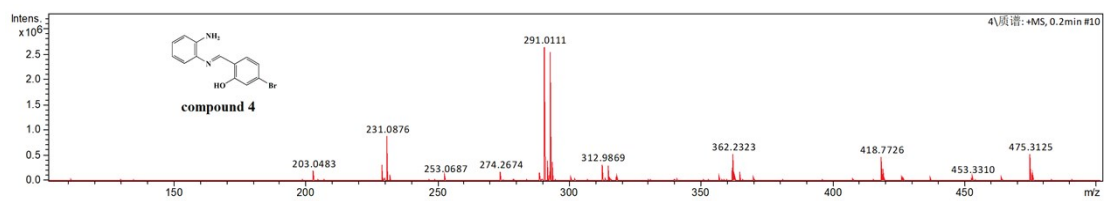^{13}C NMR spectrum of APMP-2 in DMSO-d6.

High-resolution mass spectra (HRMS) of APMP-2.
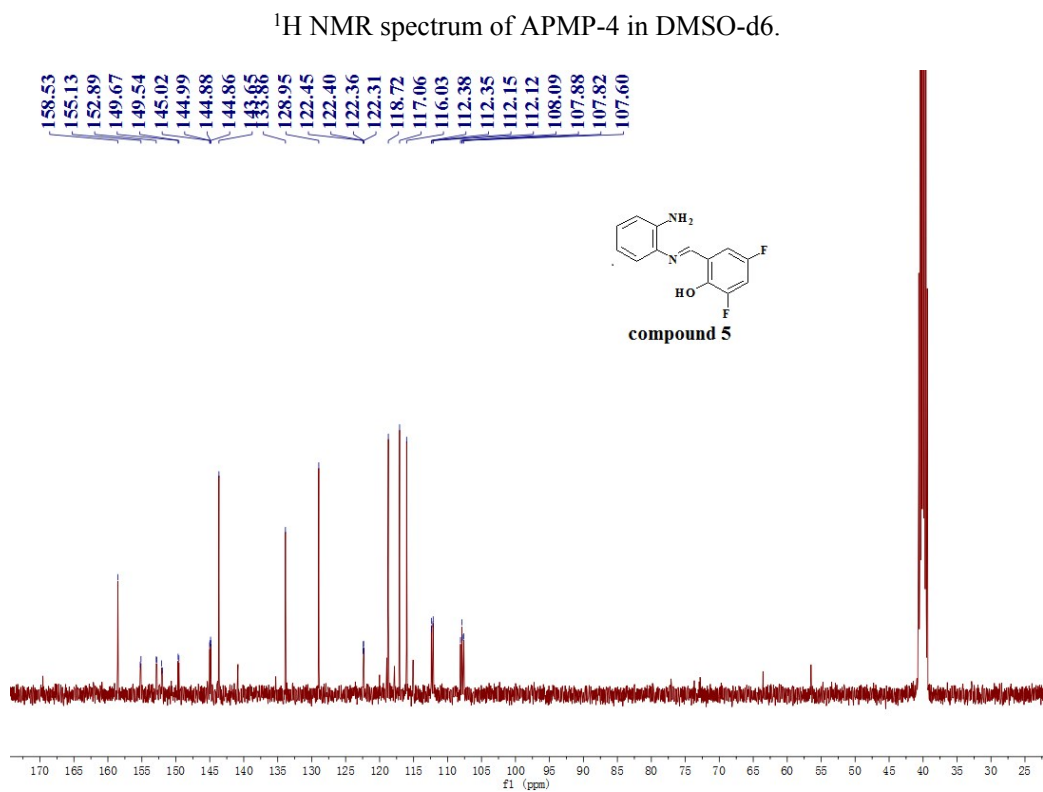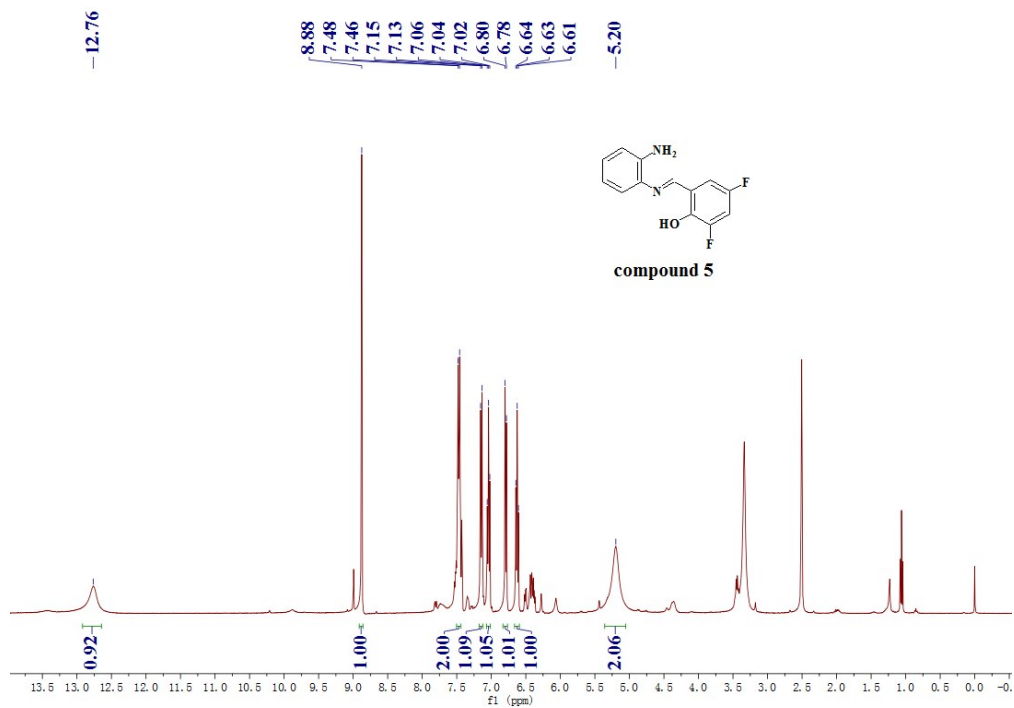
^{1}H NMR spectrum of APMP-3 in DMSO-d6.

^{13}C NMR spectrum of APMP-3 in DMSO-d6.

High-resolution mass spectra (HRMS) of APMP-3.

^{1}H NMR spectrum of APMP-4 in DMSO-d6.

^{13}C NMR spectrum of APMP-4 in DMSO-d6.
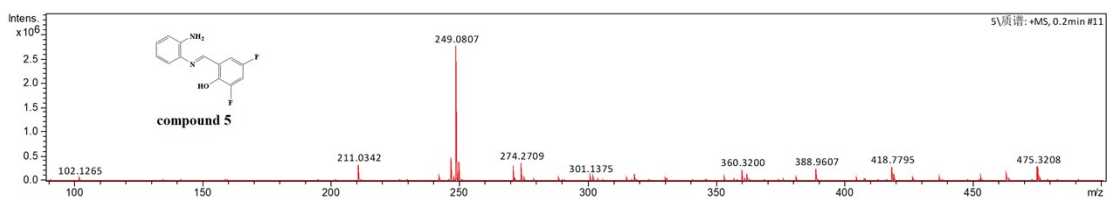

High-resolution mass spectra (HRMS) of APMP-4.

^{1}H NMR spectrum of APMP-5 in DMSO-d6.

^{13}C NMR spectrum of APMP-5 in DMSO-d6.

High-resolution mass spectra (HRMS) of APMP-5.

^{1}H NMR spectrum of APMP-6 in DMSO-d6.

^{13}C NMR spectrum of APMP-6 in DMSO-d6.

High-resolution mass spectra (HRMS) of APMP-6.

^{1}H NMR spectrum of APMP-7 in DMSO-d6.

^{13}C NMR spectrum of APMP-7 in DMSO-d6.

High-resolution mass spectra (HRMS) of APMP-7.
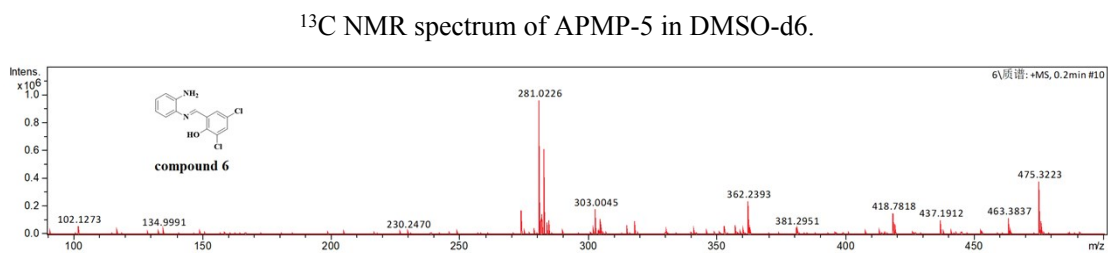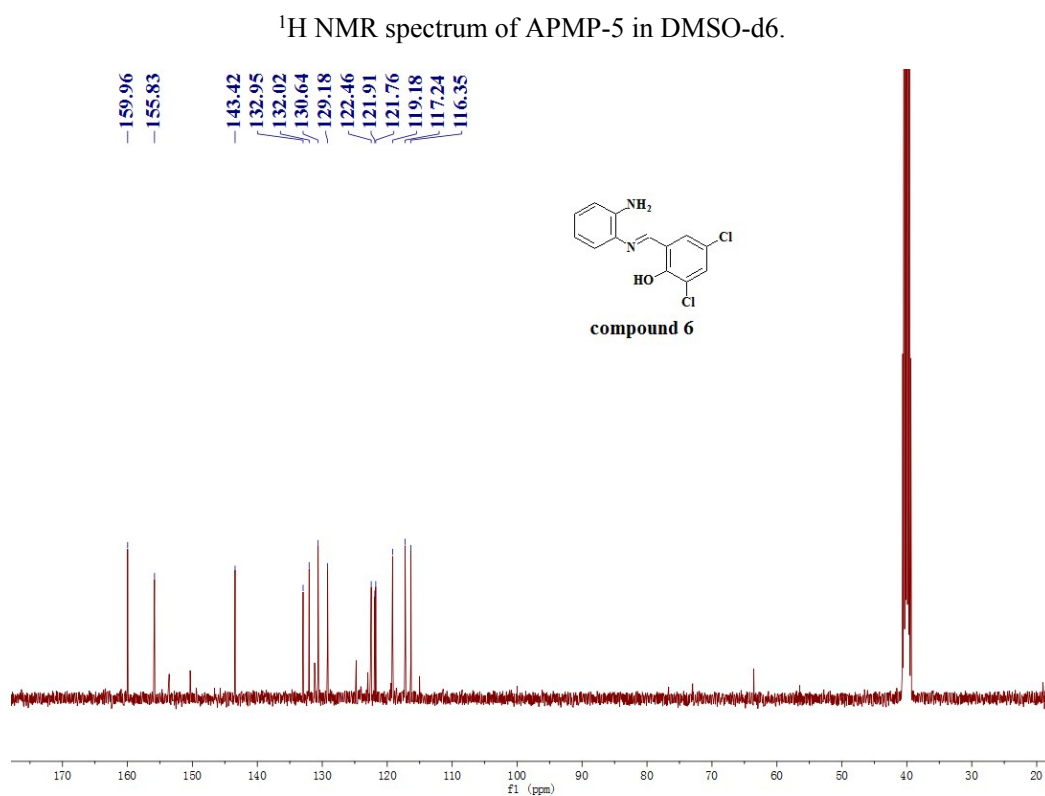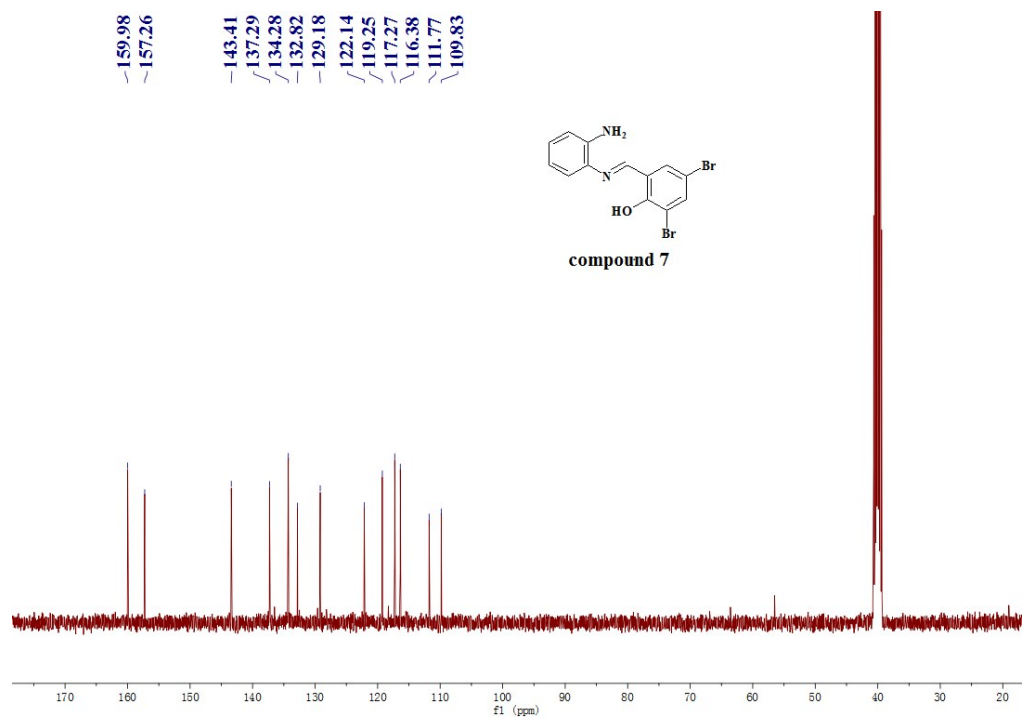
^{1}H NMR spectrum of APMP-8 in DMSO-d6.
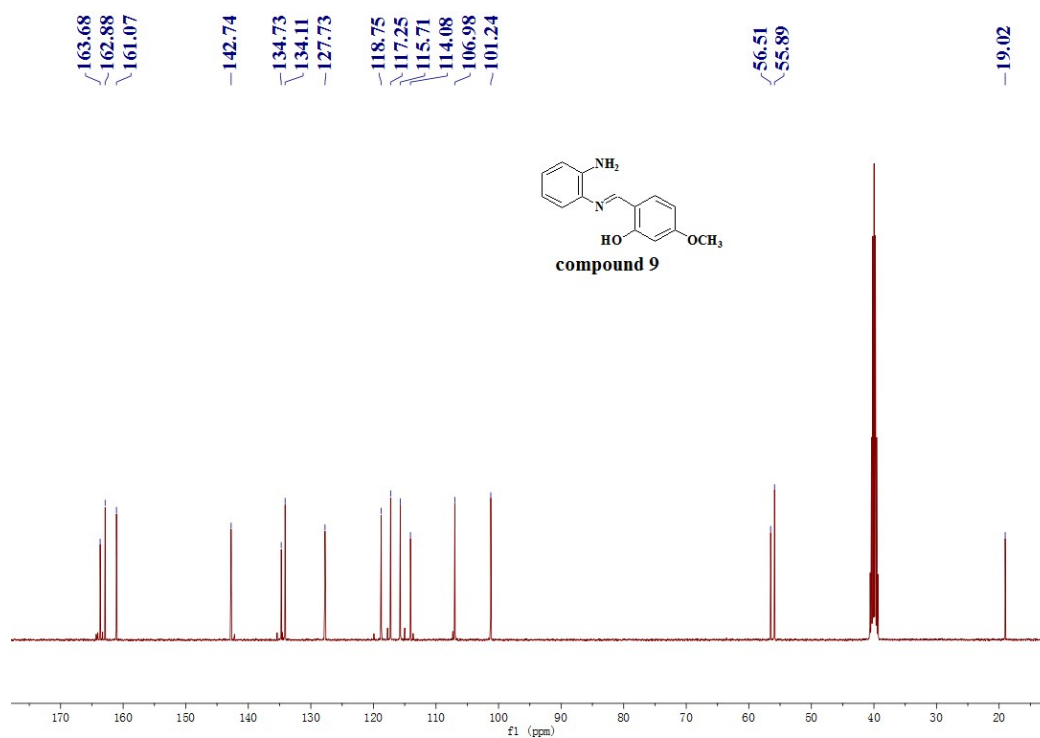
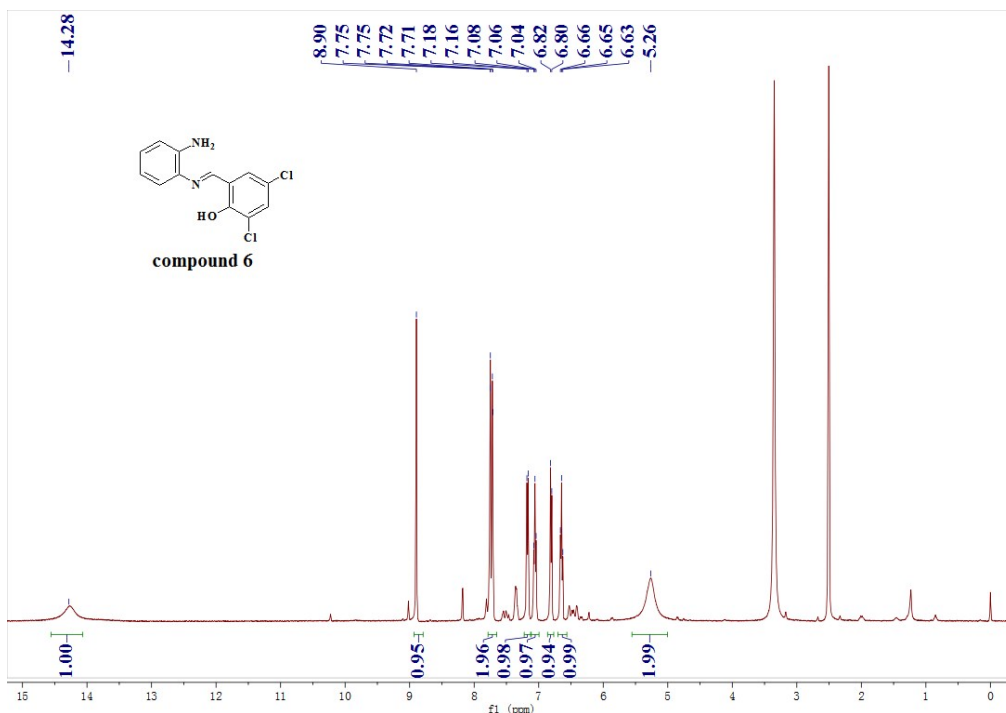

^{13}C NMR spectrum of APMP-8 in DMSO-d6.

High-resolution mass spectra (HRMS) of APMP-8.

^{1}H NMR spectrum of APMP-9 in DMSO-d6.

^{13}C NMR spectrum of APMP-9 in DMSO-d6.

High-resolution mass spectra (HRMS) of APMP-9.

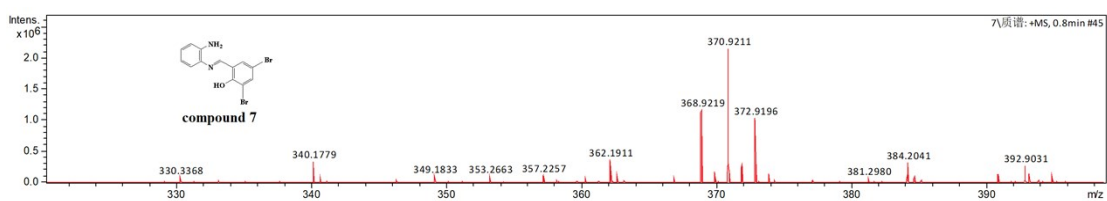14

^{1}H NMR spectrum of APMP-10 in DMSO-d6.

^{13}C NMR spectrum of APMP-10 in DMSO-d6.

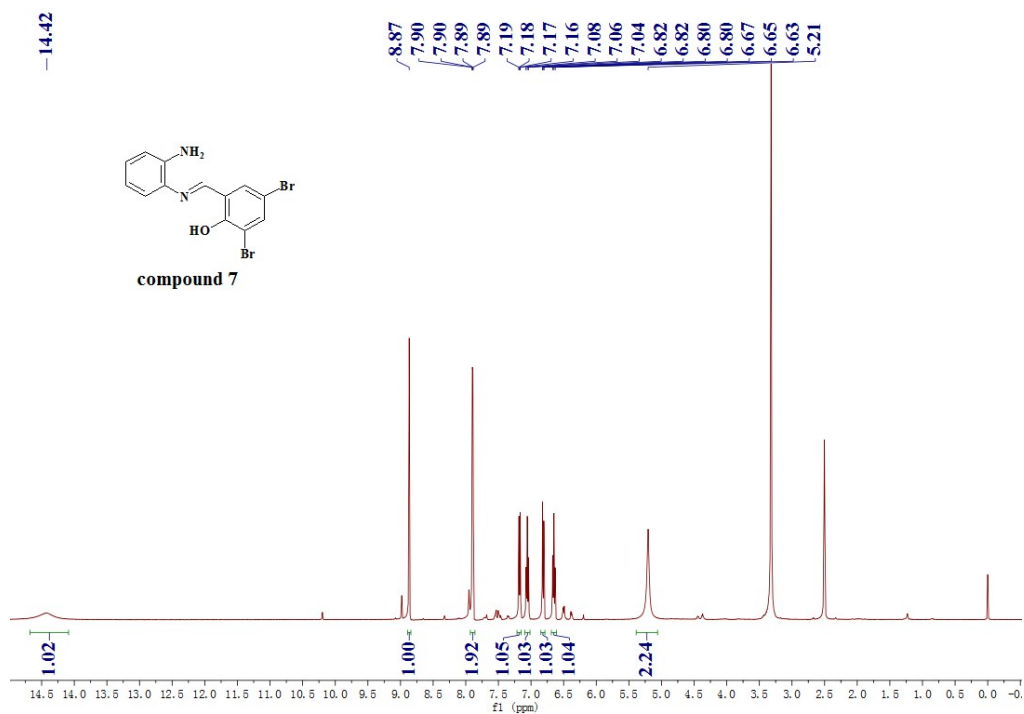
High-resolution mass spectra (HRMS) of APMP-10.

^{1}H NMR spectrum of APMP-11 in DMSO-d6.

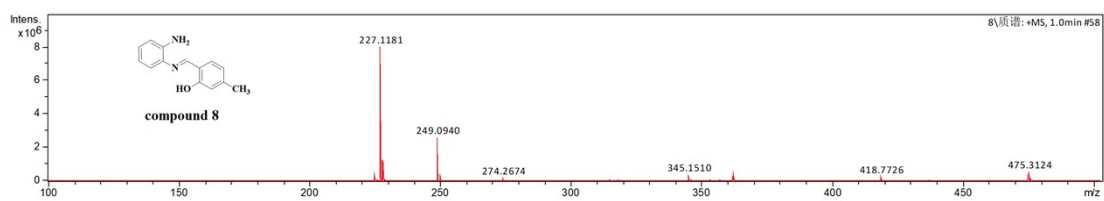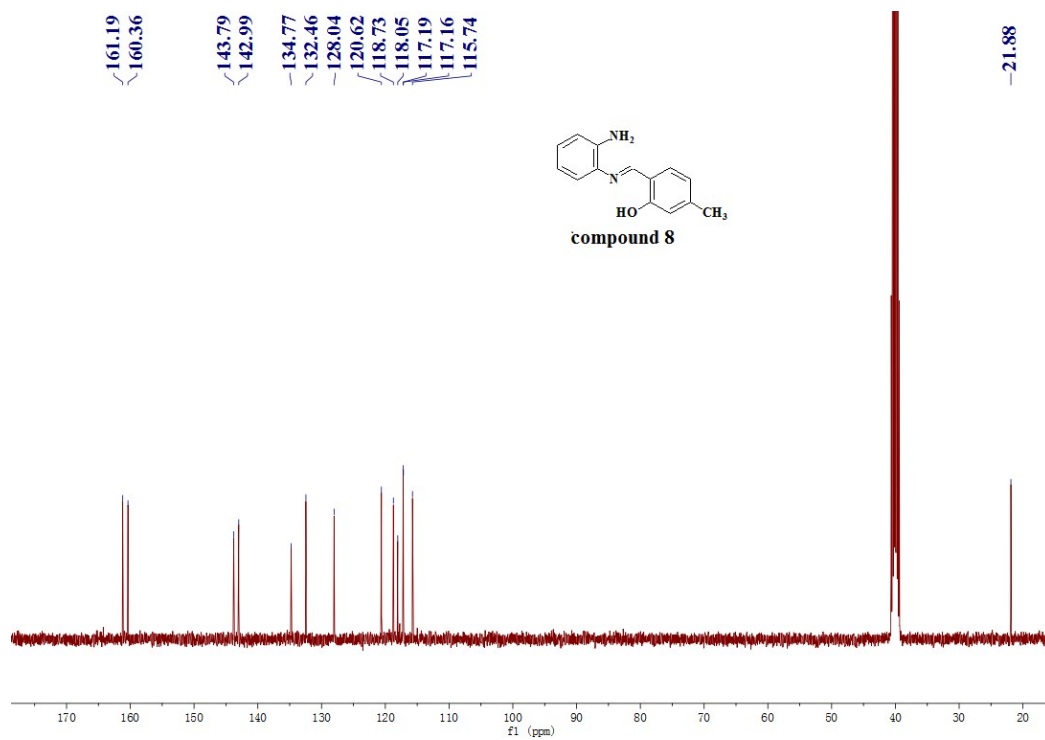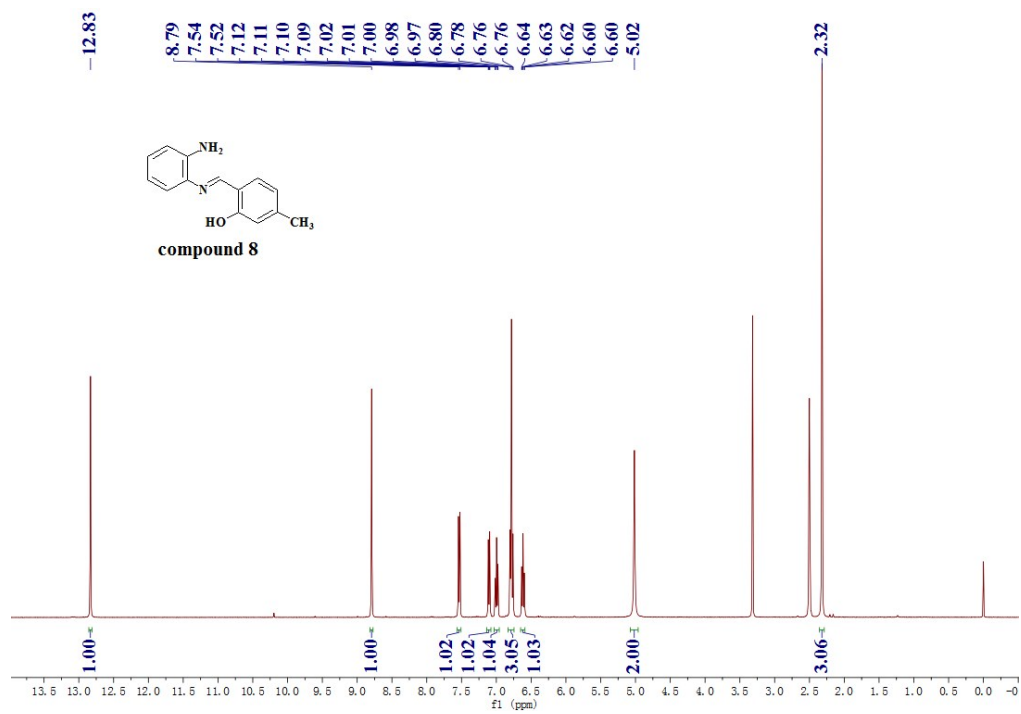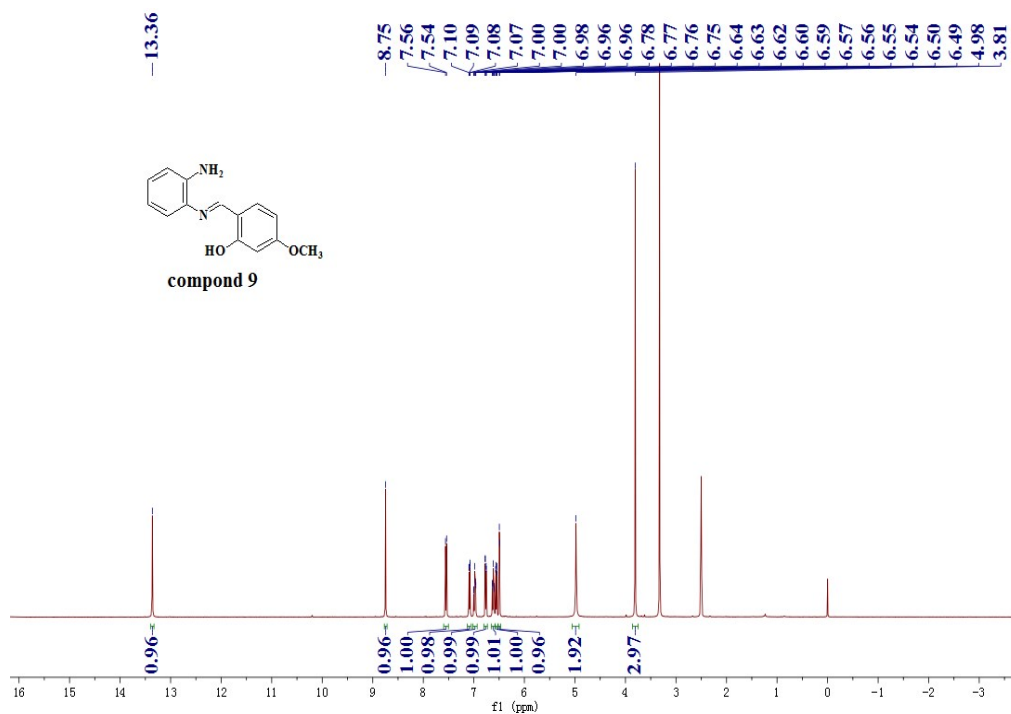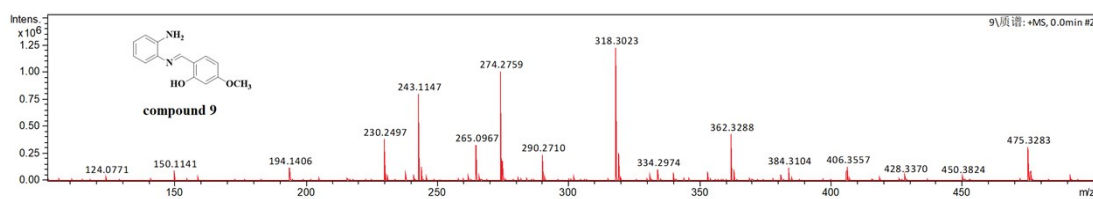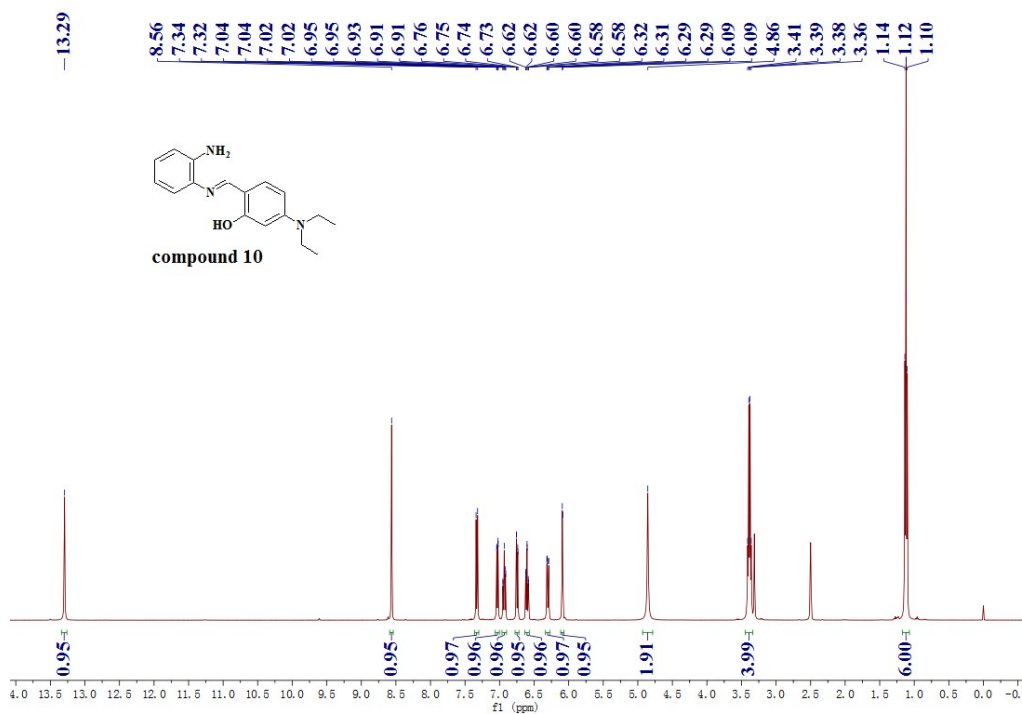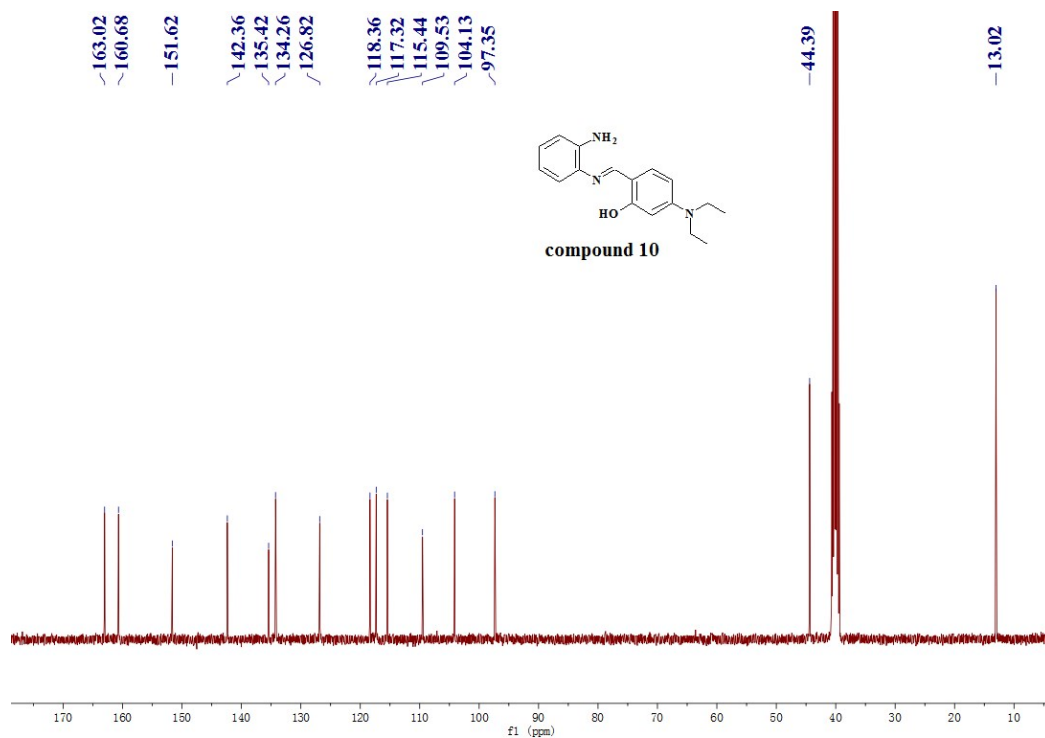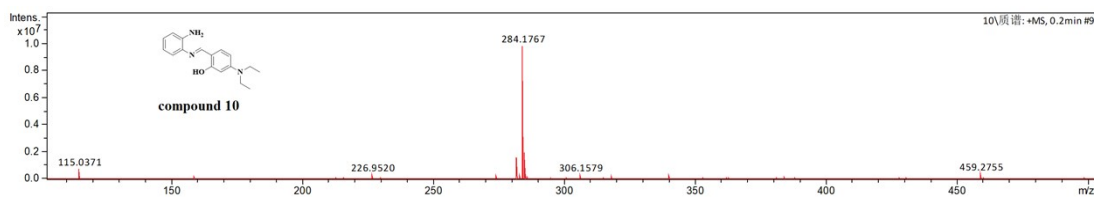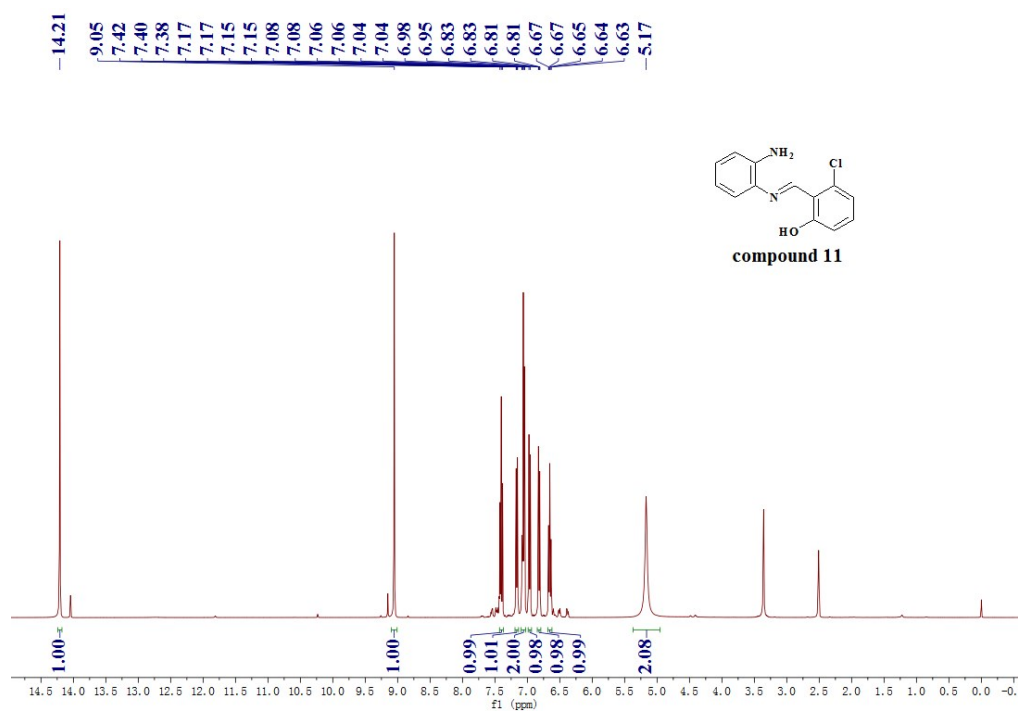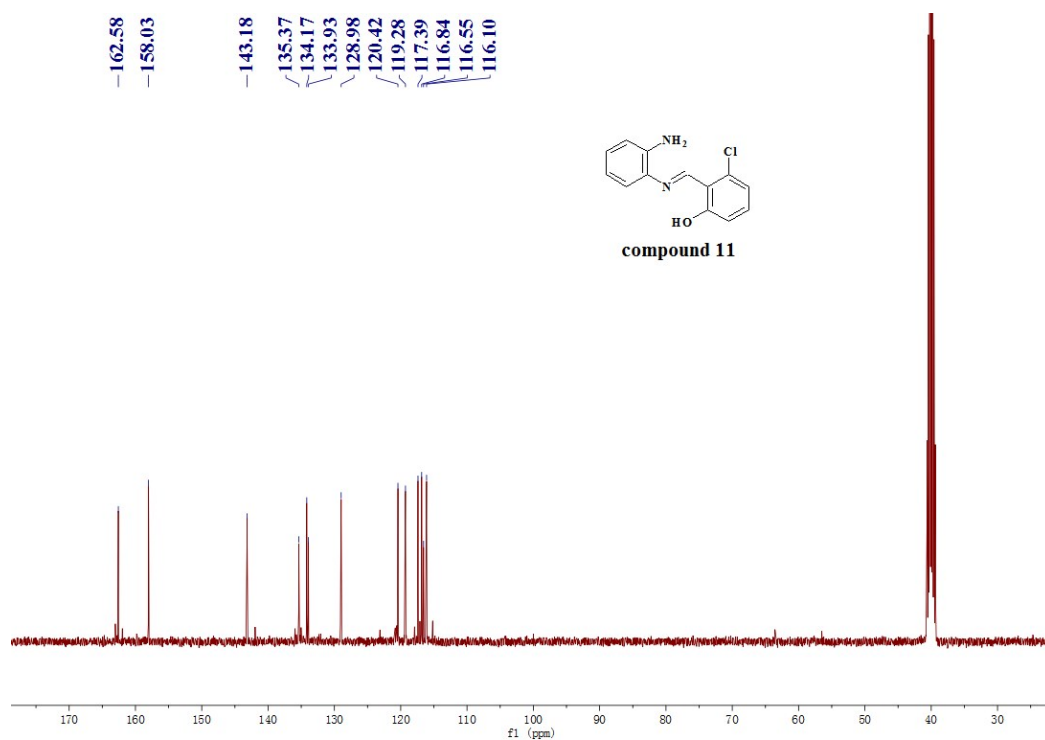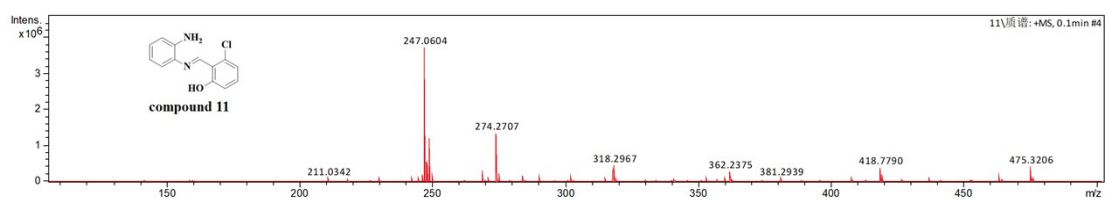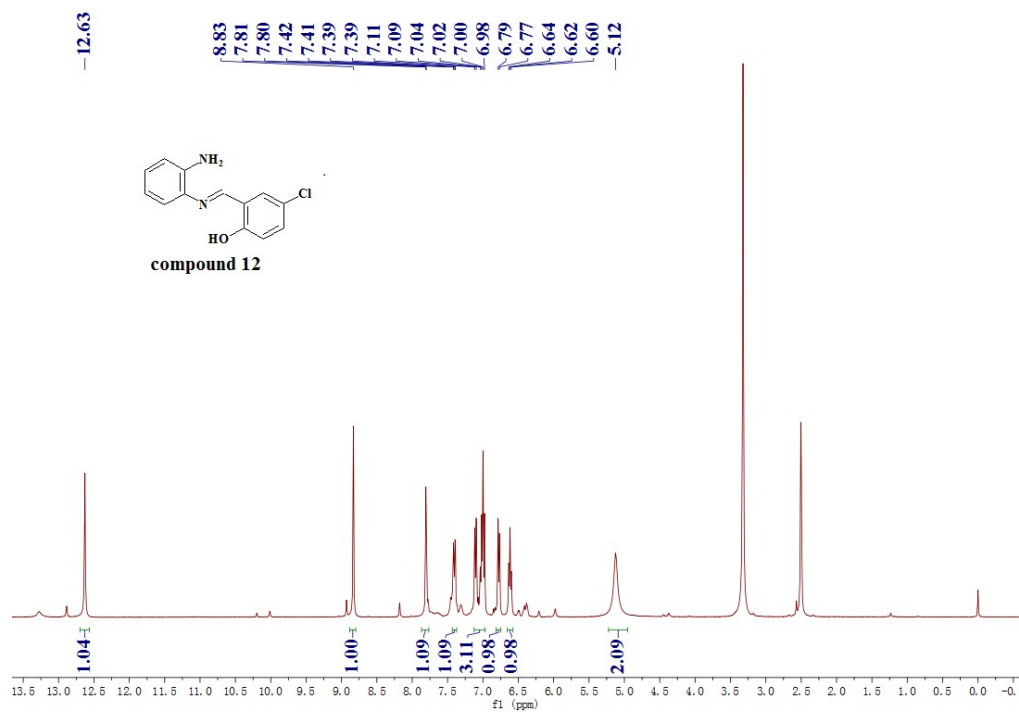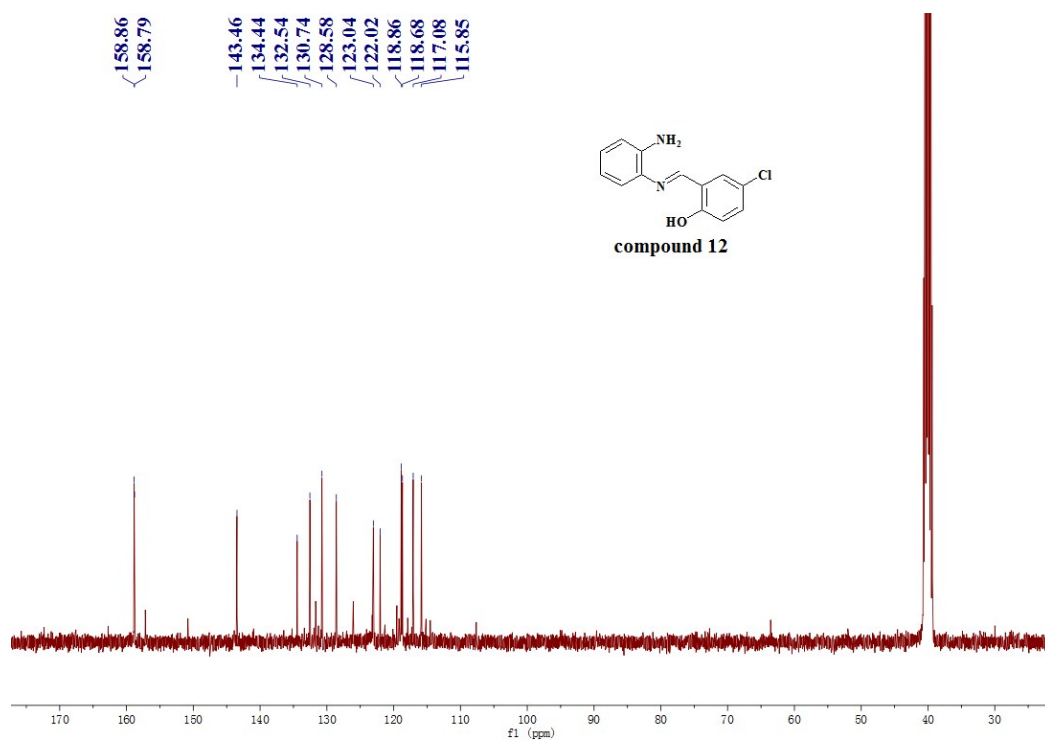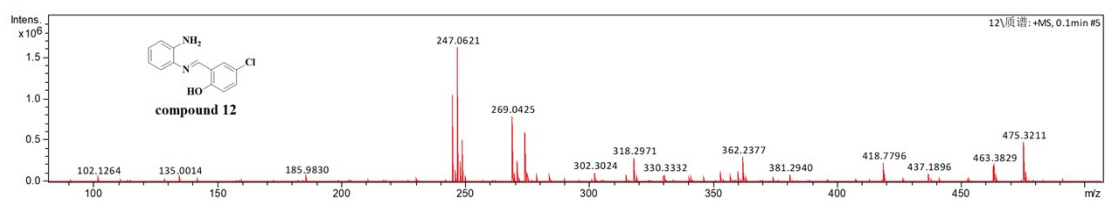^{13}C NMR spectrum of APMP-11 in DMSO-d6.

High-resolution mass spectra (HRMS) of APMP-11.

Table S1 The FL properties of APMP and its derivatives.

Compd.	R^2	R^3	R^4	R^5	λ_{ex}[nm]	λ_{em}[nm]	Δ_{H2O}[nm]	In[a.u.]	Φ_F[%]	$\tau[k_r, k_{nr}]$ ns[ns^{-1}, ns^{-1}]
APMP-1	—	—	F	—	363	478	115	472	13.58	0.78 [0.17,1.11]
APMP-2	—	—	$N(CH_2CH_3)_2$	—	362	499	137	658	4.85	0.74 [0.07,1.29]
APMP-3	—	—	CH_3	—	377	505	128	445	19.19	0.78 [0.25,1.04]
APMP-4	—	—	OCH_3	—	346	511	165	313	7.11	0.79 [0.09,1.18]
APMP-5	—	Cl	—	—	365	517	152	151	6.06	1.38 [0.04,0.68]
APMP	—	—	—	—	390	523	133	229	23.69	0.10 [2.37,7.63]
APMP-6	—	—	Cl	—	382	525	143	401	27.56	0.84 [0.33,0.86]
APMP-7	—	F	—	F	393	528	135	319	5.23	1.07 [0.05,0.89]
APMP-8	—	—	Br	—	387	535	136	222	23.9	0.96 [0.25,0.79]
APMP-9	Cl	—	—	—	376	543	167	114	15.97	1.12 [0.14,0.75]
APMP-10	—	Cl	—	Cl	446	563	117	271	17.74	0.97 [0.18,0.85]
APMP-11	—	Br	—	Br	372	574	202	123	1.21	0.88 [0.01,1.12]

The quantum yield (ΦF) and lifetime of APMP and its derivatives were investigated by using the time-resolved fluorescence spectroscopy and calibrated integrating sphere of absolute method, respectively. We found that the different positions of substituents on the benzene ring also have great influence on the fluorescence properties of the developed AIEgens. As shown in Table S1, the ΦF and fluorescence lifetime of APMP and its derivatives differ greatly from each other, and the substituting position of the same group on benzene ring also has a great influence on the fluorescence properties of AIEgens. Contrary to the above phenomenon, there is discernible regularity in the radiation and non-radiation rates of ketones calculated from ΦF and fluorescence lifetime, and it could be observed that the ΦF of the electron-withdrawing groups are basically higher than that of the electron-donating groups.
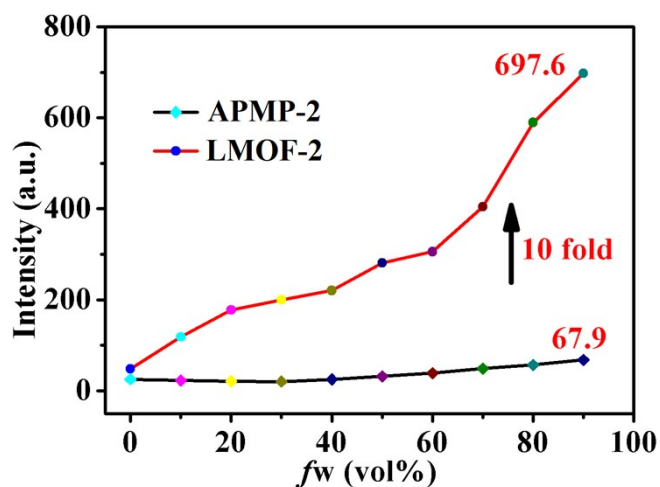
Figure S7 The enhanced fluorescence intensities of APMP-2/ZIF-8, and a fluorescence intensity

of APMP-2/ZIF-8 over 10 times the original fluorescence of APMP-2 was observed when the
water fraction reached 90%.

3. Molecular geometries of APMP derivatives in the ground (S_0) and excited (S_1).
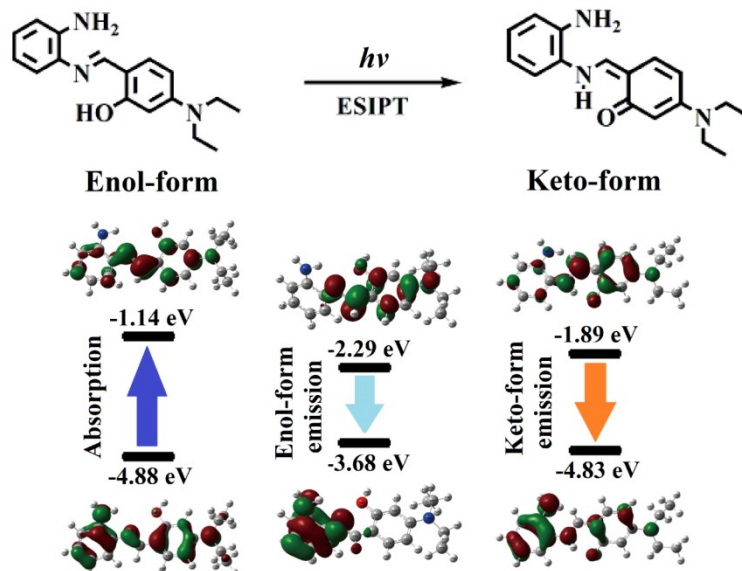
Figure S8 Molecular orbitals and energy levels of APMP-2 in the ground (S_0) and
excited (S_1) states for enol and keto forms calculated with TD-DFT at the level of
B3LYP/6-31G* based on solvation of water.
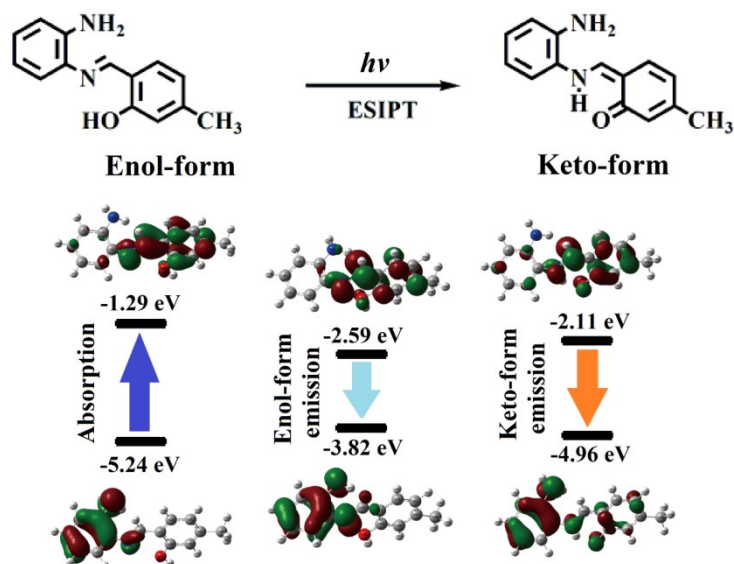
Figure S9 Molecular orbitals and energy levels of APMP-3 in the ground (S_0) and
excited (S_1) states for enol and keto forms calculated with TD-DFT at the level of
B3LYP/6-31G* based on solvation of water.
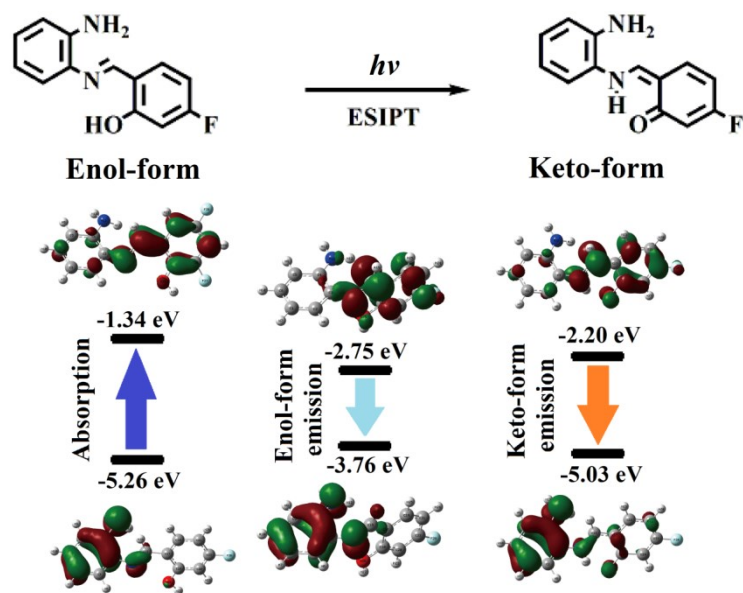
Figure S10 Molecular orbitals and energy levels of APMP-1 in the ground (S_0) and excited (S_1) states for enol and keto forms calculated with TD-DFT at the level of B3LYP/6-31G* based on solvation of water.
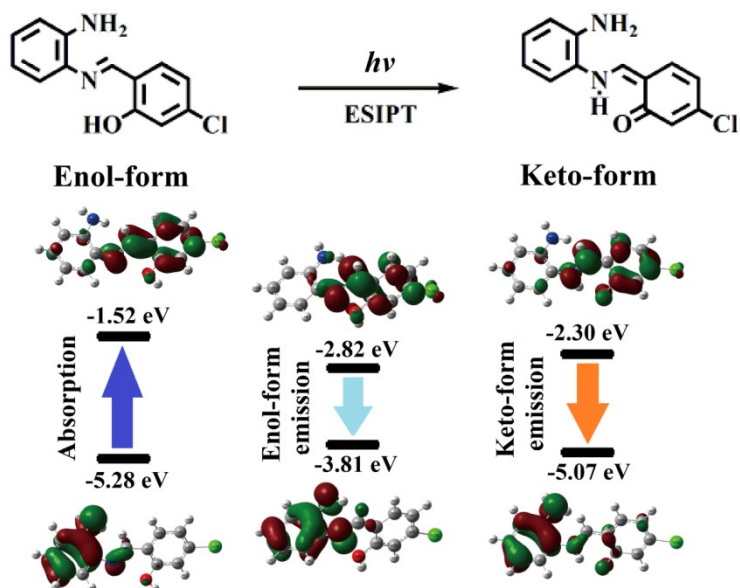
Figure S11 Molecular orbitals and energy levels of APMP-7 in the ground (S_0) and excited (S_1) states for enol and keto forms calculated with TD-DFT at the level of B3LYP/6-31G* based on solvation of water.
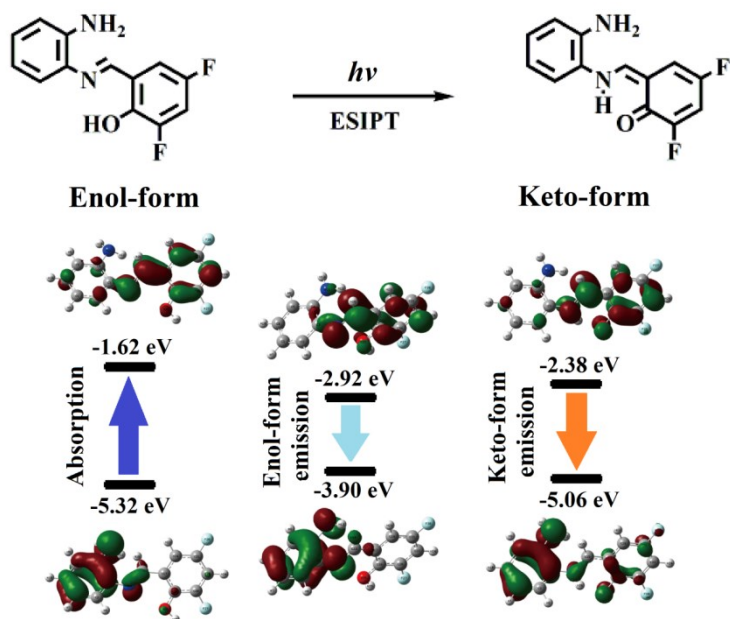
Figure S12 Molecular orbitals and energy levels of APMP-8 in the ground (S$_0$) and excited (S$_1$) states for enol and keto forms calculated with TD-DFT at the level of B3LYP/6-31G* based on solvation of water.

Figure S13 Molecular orbitals and energy levels of APMP-11 in the ground (S$_0$) and excited (S$_1$) states for enol and keto forms calculated with TD-DFT at the level of B3LYP/6-31G* based on solvation of water.

4. Molecular frontier orbitals and detail calculation data

Table S2 The frontier orbital energy levels of Enol-form, Keto-form, and the energy gap of

APMP-2, APMP-3, APMP-4, APMP-1, APMP-7, APMP-8, APMP-11.

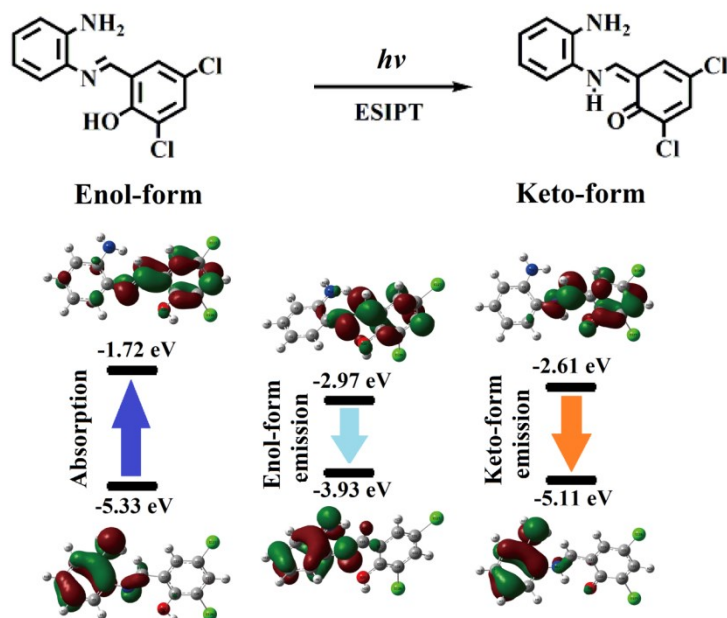| AIEgens	Energy level (HOMO)	Energy level (LUMO)	Energy gap
APMP-2	-4.88	-1.14	3.74
Enol-form	-3.68	-2.29	1.39
Keto-form	-4.83	-1.89	2.94
APMP-3	-5.24	-1.29	3.95
Enol-form	-3.82	-2.59	1.23
Keto-form	-4.96	-2.11	2.85
APMP-4	-5.26	-1.38	3.88
Enol-form	-3.76	-2.76	1.00
Keto-form	-4.99	-2.18	2.81
APMP-1	-5.28	-1.52	3.76
Enol-form	-3.81	-2.82	0.99
Keto-form	-5.07	-2.30	2.77
APMP-7	-5.26	-1.34	3.92
Enol-form	-3.76	-2.75	1.01
Keto-form	-5.03	-2.20	2.83
APMP-8	-5.32	-1.62	3.70
Enol-form	-3.90	-2.92	0.98
Keto-form	-5.06	-2.38	2.68
APMP-11	-5.33	-1.72	3.61
Enol-form	-3.93	-2.97	0.96
Keto-form	-5.11	-2.61	2.50

Table S3 Calculation data of APMP-2, APMP-3, APMP-4, APMP-1, APMP-7, APMP-8, APMP-

11 in S_0 state. [a]

AIEgen	States	Configurations	E (eV)	λ (nm)	f_{os}
APMP-2	S_{01}	H→L（92.26%）	3.28	378.07	0.89
	S_{02}	H-1→L(89.80%),H→L(6.46%)	3.87	320.02	0.35
	S_{03}	H-2→L（59.49%）	4.27	290.41	0.00
APMP-3	S_{01}	H→L（96.91%）	3.19	389.11	0.13
	S_{02}	H-1→L（58.68%）	4.12	301.05	0.09
	S_{03}	H-2→L(58.39%),H-1→L(30.97%)	4.23	293.19	0.15
APMP-4	S_{01}	H→L（97.02%）	3.15	393.58	0.17
	S_{02}	H-1→L(66.95%),H-3→L(4.99%)	4.07	304.85	0.08
	S_{03}	H-2→L(66.31%),H-1→L(24.74%)	4.20	294.99	0.12
APMP-1	S_{01}	H→L（97.18%）	3.06	404.93	0.19

		Configurations	E (eV)	λ (nm)	f_{OS}
	S_{02}	H-1→L(77.52%),H-2→L(13.92%)	3.98	311.51	0.09
	S_{03}	H-2→L（72.10%）	4.24	292.18	0.21
APMP-7	S_{01}	H→L（97.00%）	3.18	389.75	0.16
	S_{02}	H-1→L(72.20%),H-2→L(18.61%)	4.11	301.85	0.06
	S_{03}	H-2→L(64.99%),H→L+1(6.00%)	4.35	285.11	0.19
APMP-8	S_{01}	H→L（97.21%）	3.03	409.08	0.21
	S_{02}	H-1→L（72.17%）	3.91	317.09	0.11
	S_{03}	H-2→L(68.99%),H-1→L(22.23%)	4.02	308.67	0.06
APMP-11	S_{01}	H→L（97.43%）	2.95	420.84	0.20
	S_{02}	H-1→L(81.18%),H-2→L(9.71%)	3.85	322.29	0.09
	S_{03}	H-2→L(77.06%),H→L+1(6.17%)	4.04	306.74	0.09

[a] Calculated with TD-DFT at the level of B3LYP/6-31G* based on solvation of water, in which the vertical excitation as linear response solvation was used. S_{01} , S_{02} and S_{03} denoted the first and second vertical transition from S_0 state to S_1, S_2 and S_3 states, respectively, and f_{os} denoted oscillator strength of vertical transition.

Table S4 Calculation data of APMP-2, APMP-3, APMP-4, APMP-1, APMP-7, APMP-8, APMP-11 in S_1 state. [a]

AIEgen	Form	Configurations	E (eV)	λ (nm)	f_{OS}
APMP-2	Enol	H→L（98.79%）	0.51	/	0.00
	Keto	H→L（98.84%）	2.39	519.44	0.86
APMP-3	Enol	H→L（~100%）	0.25	/	0.00
	Keto	H→L（99.19%）	2.27	546.38	0.52
APMP-4	Enol	H→L（~100%）	0.06	/	0.00
	Keto	H→L（99.16%）	2.24	553.88	0.46
APMP-1	Enol	H→L（~100%）	0.06	/	0.00
	Keto	H→L（99.21%）	2.20	563.07	0.44
APMP-7	Enol	H→L（~100%）	0.06	/	0.00
	Keto	H→L（99.28%）	2.38	521.26	0.44
APMP-8	Enol	H→L（99.24%）	0.07	/	0.00
	Keto	H→L（99.16%）	2.19	565.77	0.48

APMP-11	Enol	H→L（98.78%）	0.07	/	0.00
	Keto	H→L（99.24%）	2.12	585.03	0.38

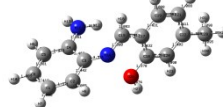[a] Calculated with TD-DFT at the level of B3LYP/6-31G* based on solvation of water, in which the vertical excitation as linear response solvation was used. f_{os} was denoted oscillator strength of the first vertical irradiation for enol-form or keto-form.

Table S5 The specific bond lengths and dihedral angles of APMP-2 in S_0 and S_1 states. [a]

	Enol-form@S_0	Enol-form@S_1	Keto-form@S_1
O_{40}-H_{41}	0.974	0.974	/
N_{14}-H_{40}	3.803	3.790	1.036
C_4–C_3–N_{14}–C_{15}	148.304	-177.823	23.328
C_3–N_{14}–C_{15}–C_{17}	176.961	96.357	-169.592
N_{14}–C_{15}–C_{17}–C_{18}	-0.622	-2.925	1.095
C_{15}–C_{17}–C_{18}–O_{40}	0.013	-2.507	0.523
C_{17}–C_{18}–O_{40}–H_{41}	-179.850	178.024	/

[a] Calculated with TD-DFT at the level of B3LYP/6-31G* based on solvation of water. The units of bond lengths and dihedral angles are Å and degree, respectively.

Table S6 The specific bond lengths and dihedral angles of APMP-3 in S_0 and S_1 states. [a]

	Enol-form@S_0	Enol-form@S_1	Keto-form@S_1
O_{40}-H_{41}	0.974	0.974	/
N_{14}-H_{40}	3.799	3.782	3.782
C_4–C_3–N_{14}–C_{15}	-179.850	2.103	32.782
C_3–N_{14}–C_{15}–C_{17}	-179.570	-103.330	-172.395
N_{14}–C_{15}–C_{17}–C_{18}	2.723	15.691	3.684
C_{15}–C_{17}–C_{18}–O_{40}	0.360	0.984	0.899
C_{17}–C_{18}–O_{40}–H_{41}	178.532	-178.858	/

[a] Calculated with TD-DFT at the level of B3LYP/6-31G* based on solvation of water. The units of bond lengths and dihedral angles are Å and degree, respectively.

Table S7 The specific bond lengths and dihedral angles of APMP-4 in S_0 and S_1 states. [a]

	Enol-form@S_0	Enol-form@S_1	Keto-form@S_1
O_{40}-H_{41}	0.974	0.973	/
N_{14}-H_{40}	3.790	3.774	1.033
C_4–C_3–N_{14}–C_{15}	54.688	2.120	33.492
C_3–N_{14}–C_{15}–C_{17}	-179.695	-102.157	-170.054
N_{14}–C_{15}–C_{17}–C_{18}	1.205	17.413	3.805
C_{15}–C_{17}–C_{18}–O_{40}	-0.099	0.269	-0.018
C_{17}–C_{18}–O_{40}–H_{41}	179.852	178.018	/

[a] Calculated with TD-DFT at the level of B3LYP/6-31G* based on solvation of water. The units

of bond lengths and dihedral angles are Å and degree, respectively.

Table S8 The specific bond lengths and dihedral angles of APMP-1 in S_0 and S_1 states. [a]

	Enol-form@S_0	Enol-form@S_1	Keto-form@S_1
O_{40}-H_{41}	0.974	0.973	/
N_{14}-H_{40}	3.781	3.758	1.031
C_4–C_3–N_{14}–C_{15}	52.67309	1.7644	41.72782
C_3–N_{14}–C_{15}–C_{17}	-179.88614	-100.38991	-178.68744
N_{14}–C_{15}–C_{17}–C_{18}	2.50728	12.90955	3.35026
C_{15}–C_{17}–C_{18}–O_{40}	0.11369	-1.15782	0.54082
C_{17}–C_{18}–O_{40}–H_{41}	179.04552	-177.47064	/

[a] Calculated with TD-DFT at the level of B3LYP/6-31G* based on solvation of water. The units

of bond lengths and dihedral angles are Å and degree, respectively.

Table S9 The specific bond lengths and dihedral angles of APMP-7 in S_0 and S_1 states. [a]

	Enol-form@S_0	Enol-form@S_1	Keto-form@S_1

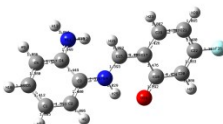|			
O$_{40}$-H$_{41}$	0.974	0.973	/
N$_{14}$-H$_{40}$	3.786	3.772	1.029
C$_4$–C$_3$–N$_{14}$–C$_{15}$	56.428	2.764	36.930
C$_3$–N$_{14}$–C$_{15}$–C$_{17}$	-179.785	-102.817	-174.527
N$_{14}$–C$_{15}$–C$_{17}$–C$_{18}$	1.946	16.181	2.779
C$_{15}$–C17–C$_{18}$–O$_{40}$	0.162	-0.768	0.165
C$_{17}$–C18–O$_{40}$–H$_{41}$	179.026	-179.462	/

a) Calculated with TD-DFT at the level of B3LYP/6-31G* based on solvation of water. The units

of bond lengths and dihedral angles are Å and degree, respectively.

Table S10 The specific bond lengths and dihedral angles of APMP-8 in S$_0$ and S$_1$ states. [a]

	Enol-form@S$_0$	Enol-form@S$_1$	Keto-form@S$_1$
O$_{40}$-H$_{41}$	0.975	0.975	/
N$_{14}$-H$_{40}$	3.802	3.789	1.031
C$_4$–C$_3$–N$_{14}$–C$_{15}$	45.87178	2.02539	39.07799
C$_3$–N$_{14}$–C$_{15}$–C$_{17}$	179.77356	-100.41746	-173.75028
N$_{14}$–C$_{15}$–C$_{17}$–C$_{18}$	1.31516	12.49268	3.74114
C$_{15}$–C$_{17}$–C$_{18}$–O$_{40}$	0.04738	0.07607	0.59029
C$_{17}$–C$_{18}$–O$_{40}$–H$_{41}$	179.34455	-179.87095	/

a) Calculated with TD-DFT at the level of B3LYP/6-31G* based on solvation of water. The units

of bond lengths and dihedral angles are Å and degree, respectively.

Table S11 The specific bond lengths and dihedral angles of APMP-11 in S$_0$ and S$_1$ states. [a]

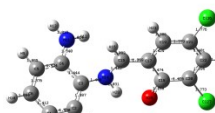|	Enol-form@S$_0$	Enol-form@S$_1$	Keto-form@S$_1$
O$_{40}$-H$_{41}$	0.976	0.975	/
N$_{14}$-H$_{40}$	3.748	3.742	1.031
C$_4$–C$_3$–N$_{14}$–C$_{15}$	47.601	2.494	67.791
C$_3$–N$_{14}$–C$_{15}$–C$_{17}$	-179.846	-100.106	154.209
N$_{14}$–C$_{15}$–C$_{17}$–C$_{18}$	3.469	12.623	-3.433
C$_{15}$–C$_{17}$–C$_{18}$–O$_{40}$	-0.088	-0.611	0.655
C$_{17}$–C$_{18}$–O$_{40}$–H$_{41}$	179.578	-179.843	/

a) Calculated with TD-DFT at the level of B3LYP/6-31G* based on solvation of water. The units

of bond lengths and dihedral angles are Å and degree, respectively.
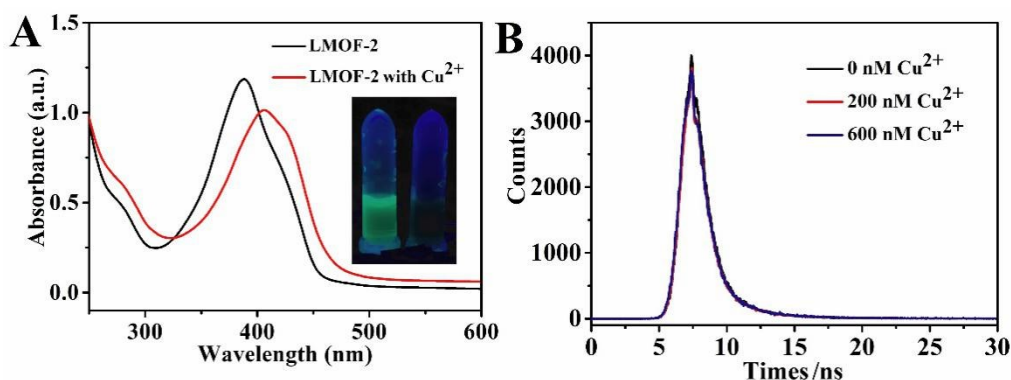
Figure S14. (A) UV-vis spectra of before (black line) and after (red line) the treatment by 50 μM Cu^{2+}; Insert: the photographs of LMOF-2 dispersion in the (left) absence and (right) presence of Cu^{2+} (400 nM) under 365 nm UV light. (B) Fluorescence decay profiles of LMOF-2 obtained by treatment with different concentrations of Cu^{2+} were 0, 200, and 600 nM.

5. Detection Cu^{2+} and application to water samples

The selectivity of the LMOF-2 FL sensing system was estimated and shown in **Figure 4A**. Besides Cu^{2+} , the effects of 15 other kinds of targets, including Mn^{2+}, Zn^{2+}, Ag$^+$, Mg^{2+}, Hg$^+$, Cd^{2+}, Pb^{2+}, glucose, glutathione, lysine, leucine, ascorbic acid, ayrosine, serine and threonine at the same concentration of Cu^{2+}, on the FL response of LMOF-2 containing 100 nM Cu^{2+} at the same time were investigated. We can find that the FL intensities are significantly quenched by 10 nM Cu^{2+}, whereas almost no additional inhibition of the FL intensities happens in the presence of others metal ion or molecules. Apparently, these results clearly indicate that the LMOF-2 FL sensing system exhibits high selectivity for Cu^{2+}.

The fluorescence intensity of LMOF-2 is sensitive to the presence of nanomolar concentrations of Cu^{2+}. To evaluate the applicability of the sensitive sensing system for Cu^{2+} ions, the dynamic range and LOD were investigated under the above-mentioned optimum experimental conditions. As shown in **Figure 4B**, the FL intensity of the LMOF-2 is quenched obviously with increasing the concentration of Cu^{2+}. There is a good response range between the quenching level, *(F$_0$ − F) /F$_0$,* and the concentration of Cu^{2+} in the range from 1 to 100 nM (see the inset view of Fig. 4B) with the following equation:

$$y = -0.442e^{\left(-\frac{\chi}{49.546}\right)} - 0.442e^{\left(-\frac{\chi}{49.547}\right)} + 0.878 \qquad R^2=0.997$$

where F_0 and F represent, respectively, the FL intensities of LMOF-2 in the absence and presence of Cu^{2+} and χ is the concentration of Cu^{2+}. The LOD of Cu^{2+} (at the ratio of signal-to-noise = 3) was calculated to be 0.55 nM. In comparison with other reported FL methods [1-19], this sensing approach also shows higher sensitivity (1 or 2 orders of magnitude decrease in LOD) for the detection of Cu^{2+}. The highly sensing sensitivity can be attributed to the AIEgens assembled on the external surface of Nanoscale ZIF-8. This design permits that the FL probe can fully interact with the target, so as to achieve the best detection effect.

Table S12 Various Sensing Strategies for the Detection of Cu^{2+}.

| Method	Material	LOD	Real samples	Ref
Colorimetric	PMTPS	3 μM	Lake water	[1]
Colorimetric	CdS QDs	5.3 nM	River water	[2]
Colorimetric	rQDs, gQDs	1.3 nM	Human urine	[3]
SERS	Cys-AuNSs	10 μM	Ionic mixture	[4]
SERS	AuNP−AgNP	0.18 nM	River water	[5]
Electrochemical	NS4s	400 nM	Rat brain	[6]
Electrochemical	TPAASH	80.3 nM	Rat brain	[7]
Electrochemical	ZnO/CdS	10 nM	River water	[8]
MRI	copper-bath	20 μM	/	[9]
DNAzyme	PLDz	21.1 nM	Ionic mixture	[10]
Click chemistry	G-quadruplex	5.9 nM	Tap water	[11]
Fluorescence	luminol-Tb-GMP CPNPs	4.2 nM	River water,ascites,urine	[12]
Fluorescence	TPM	840 nM	Human colon	[13]
Fluorescence	H39GFP	50 nM	Human urine	[14]
Fluorescence	hPEI-AgNCs	10 nM	River water	[15]
Fluorescence	GF	0.6 nM	Serum	[16]
Fluorescence	CDs	0.3 μM	Rat brain	[17]
Fluorescence	CDs@Eu-DPA MOFs	26.3 nM	Drinking water	[18]
Fluorescence	QDs/CDs@ZIF-8	1.53 nM	Tap water	[19]
Fluorescence	LMOF-2	0.55 nM	Xiangjiang river of Changsha	This work
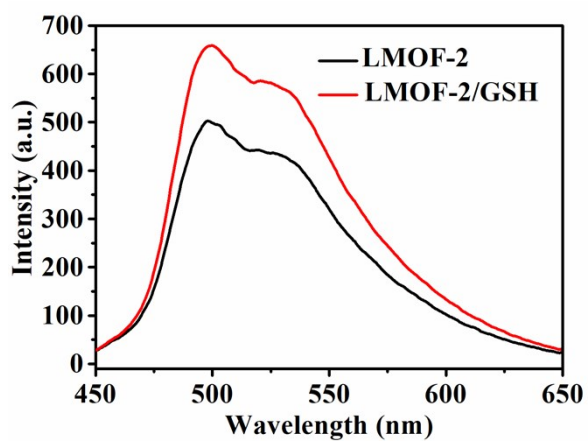
Figure S15 The FL responses of APMP-2 and LMOF-2/GSH.
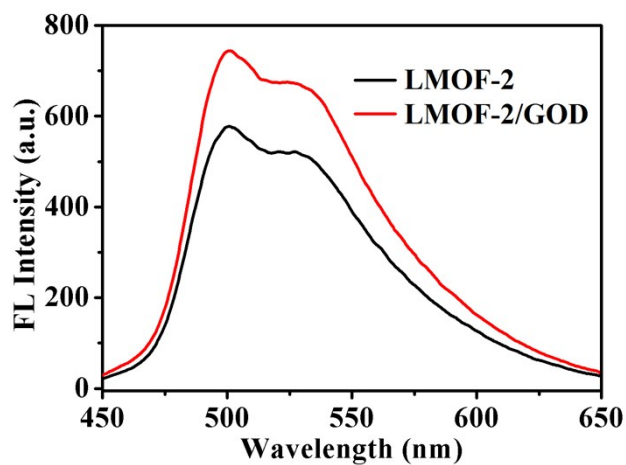

Figure S16 The FL responses of LMOF-2 and LMOF-2/GOD.
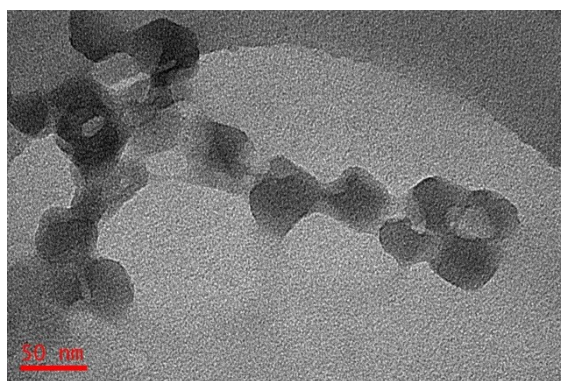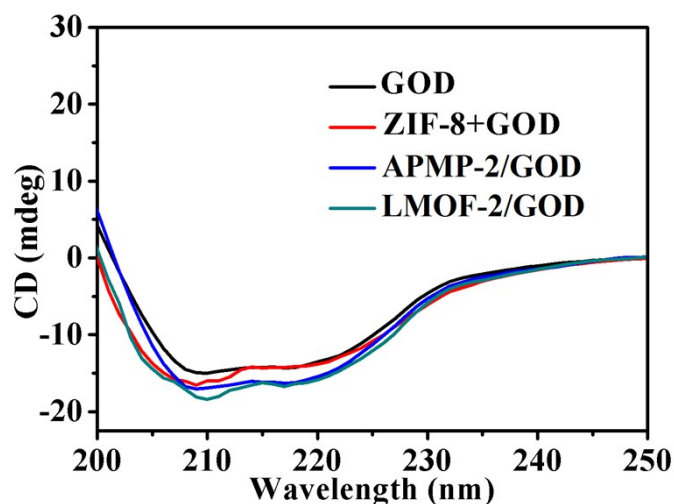

Figure S17 TEM image of LMOF-2/GOD.

6. CD spectra

Figure S18 CD spectra of GOD, ZIF-8/GOD, APMP-2/GOD and LMOF-2/GOD.

CD spectrometry is an effective method to investigate the structure variation of protein after interacting with nanoparticles. It can provide detail information about the percentages of different secondary structure, such α-helix, β-sheet, β-turn, and random coil. To inquiry the possible influence LMOF-2 and ZIF-8 on the secondary structure of GOD, the CD spectra of GOD, APMP-2/GOD and LMOF-2/GOD system were performed. As the CD spectra shown in **Figure S18**, GOD exhibits two negative absorption peaks at 208 and 222 nm which are the characteristic absorption peaks of the α-helix structure of proteins. After the addition of APMP-2, the absorbances of two negative bands at 208 and 222 nm all increase significantly, indicating the secondary structure of GOD is varied, especially for the α-helix structure. In addition, there is nearly no change between the CD spectra of APMP-2/GOD and LMOF-2/GOD, indicating that ZIF-8 had slightly effect on the secondary structure of GOD. In order to accurately quantify the α-helical structure of GOD, the results are expressed in mean residue ellipticity (MRE) (deg cm^2 dmol^{-1}) by the following equation:

$$MRE = \frac{\theta_{obs}}{10nlC_p}$$

Herein, θ_{obs} represents the measured ellipticity, n is the total number of amino acids of GOD (587), l is the path length (0.1 cm), and C_p is the concentration of GOD, respectively. Therefore, the content of the α-helix structure of GOD can be calculated through the following equation:

$$\alpha - helix = \left[\frac{- MRE_{208\,nm} - 4000}{33000 - 4000} \right] \times 100\%$$

The results of the analysis are shown in Table S12. It can be seen that the percentage of protein secondary structure of APMP-2/GOD and LMOF-2/GOD is substantially unchanged, further indicating that ZIF-8 has less influence on the secondary structure of GOD. In addition, an obvious increasing tendencies of the α-helix and β-sheet contents and decreasing tendencies of other secondary structure contents were obtained at the present of APMP-2 or APMP-2/ZIF-8, this indicates that the hydrogen bond network of the GOD becomes stronger after interaction with APMP-2, which may attribute to the formation of non-covalent bonds between the APMP-2 and the peptide bond of the GOD.

Table S13 The percentage of protein secondary structure of pure GOD, APMP-2/GOD and LMOF-2/GOD.

	α-Helix (%)	β-sheet (%)	β-Turn (%)	Random coil (%)
GOD	17.4	15.1	20.7	46.8
APMP-2/GOD	18.3	15.6	20.4	45.7
LMOF-2/GOD	18.3	16.1	20.4	45.2

7. GOD relative activity assay

The GOD activity was determined by coupling oxidation of glucose producing H_2O_2, which was further used to oxidize TMB in the presence of HRP. In a typical reaction, TMB (72 μL, 1 mg /mL), glucose (20 μL, 10 mM), HRP (5 μL, 100 μg /mL), GOD (5 μL, 100 μg /mL) were mixed, and the appropriate amount of PBS buffer (pH=6.5, 100 mM) was added to make up the volume to 500 μL. The mixture was then allowed to stand for 30 min. The absorbance was measured at 650 nm. For optimization of the HRP/GOD ratio, different ratios from 6:1 to 1:6 were used, and the abovementioned procedure was followed.

The relative activity of bio-catalysts was calculated from the formula [20, 21]

$$R = \frac{A_{IE}}{A_0} \times 100\%$$

where A_{IE} is the activity of immobilized GOD and A_0 is the activity of native GOD.
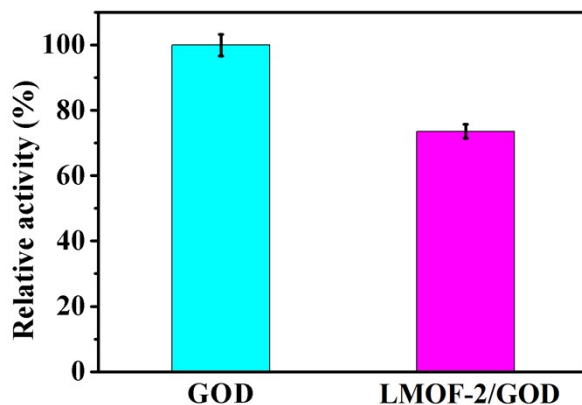
Figure S19 Relative enzymatic activity of GOD in LMOF-2/GOD.

8. Cascade reaction of enzyme catalyzed oxidation and redox ring-closure reaction
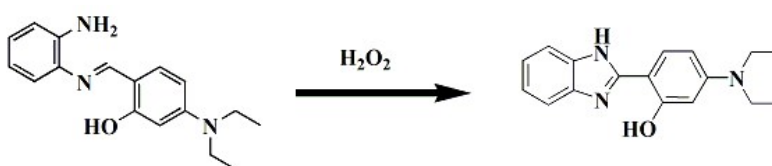

Figure S20 The redox ring-closure reaction of APMP-2 to generate the blue-shifted product 2-

(1H-Benzoimidazol-2-yl)-5-diethylamino-phenol (Compound 13)

Compound 13: ^{1}H NMR (DMSO-d_6, 400 MHz) δ 1.13 (t, J = 6.0 Hz, 6H), 3.38 (m, J = 6.0 Hz, 4H), 6.20 (s, 1H), 6.37 (d, J = 3.0 Hz, 1H), 7.20 (t, J = 3.0 Hz, 2H), 7.55 (s, 2H), 7.79 (d, J = 9.0 Hz, 1H), 12.85 (s, 2H). HRMSEI(+) calcd for $C_{17}H_{19}N_3O^+$ [M+1]$^+$ 282.1601, found 282.1593;

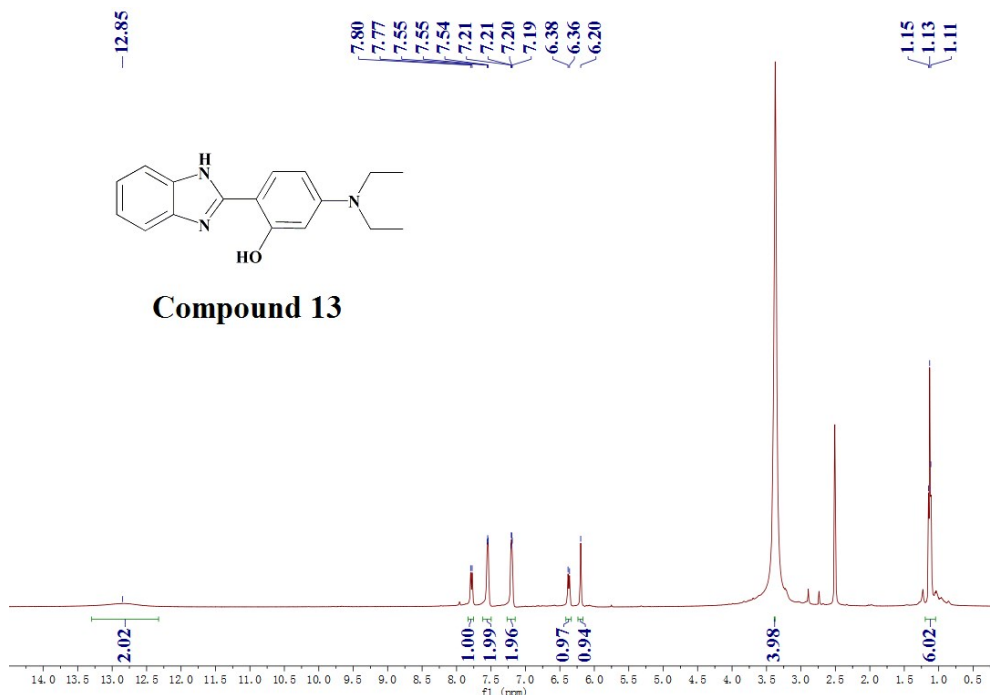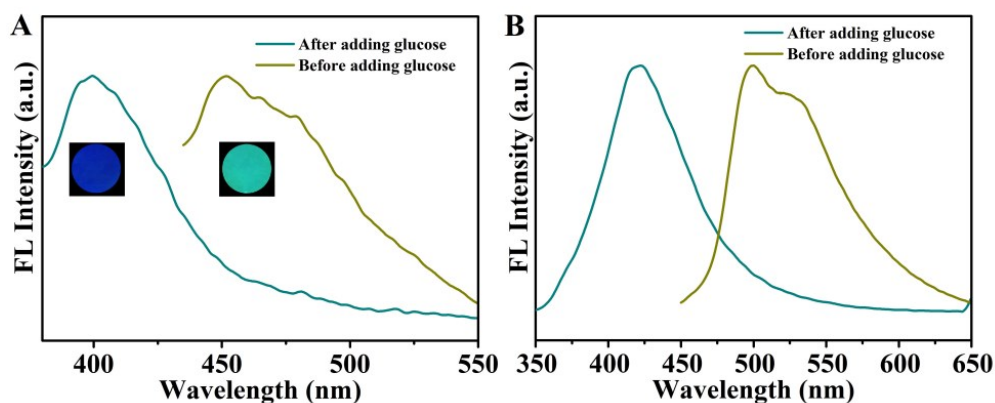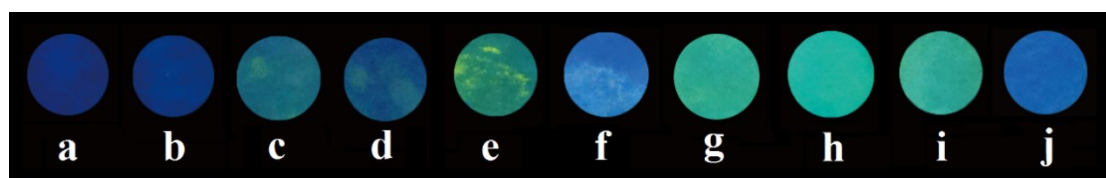**Figure S21** ^{1}H NMR spectrum of 2-(1H-Benzoimidazol-2-yl)-5-diethylamino-phenol in DMSO-

d6.

Figure S22 Fluorescence spectra of filter paper loaded with LMOFs/GOD (A) and LMOFs/GOD solution (B) before and after (ex: 333 nm em: 399 nm) being treated by glucose.

Figure S23 a) The untreated filter paper immersed in aqueous solution for 30 min. b) The untreated filter paper immersed in 10 mM glucose solution for 30 min. c) The filter paper loaded with APMP-2 and immersed in aqueous solution for 30 min. d) The filter paper loaded with APMP-2 and immersed in 10 mM glucose solution for 30 min. e) The filter paper loaded with APMP-2/GOD and immersed in aqueous solution for 30 min. f) The filter paper loaded with APMP-2/GOD and immersed in 10 mM glucose solution for 30 min. g) The filter paper loaded with LMOF-2 and immersed in aqueous solution for 30 min. h) The filter paper loaded with LMOF-2 and immersed in 10 mM glucose solution for 30 min. i) The filter paper loaded with LMOF-2/GOD and immersed in aqueous solution for 30 min. j) The filter paper loaded with LMOF-2/GOD and immersed in 10 mM glucose solution for 30 min.
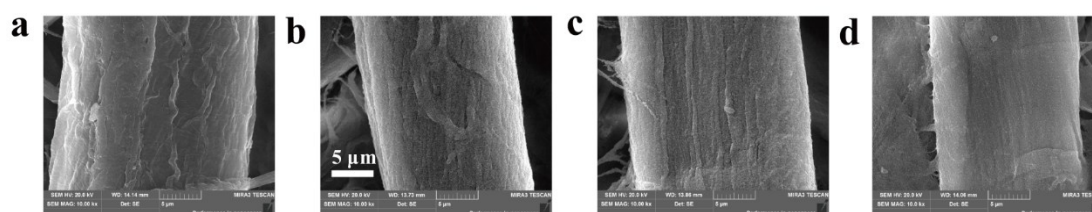
Figure S24 SEM images of the filter paper without any treatment (a) and filter paper loaded with ZIF-8 (b), APMP-2/ZIF-8 (c) and LMOF-2/GOD (d), respectively.

References

[1]   Z. Yao, Y. Yang, X. Chen, X. Hu, L. Zhang, L. Liu, Y. Zhao, H. C. Wu, *Anal. Chem.*, 2013, **85**, 5650-5653.

[2]   S. Tang, M. Wang, Z. Li, P. Tong, Q. Chen, G. Li, J. Chen, L. Zhang, *Biosens. Bioelectron.*, 2017, **89**, 866-870.

[3]   Y. Cai, J. You, Z. You, F. Dong, S. Du, L. Zhang, *Biosens. Bioelectron.*, 2018, **99**, 332-337.

[4]   P. Ndokoye, J. Ke, J. Liu, Q. Zhao, X. Li, *Langmuir*, 2014, **30**, 13491-13497.

[5]   Y. Wang, Z. Su, L. Wang, J. Dong, J. Xue, J. Yu, Y. Wang, X. Hua, M. Wang, C. Zhang, F. Liu, *Anal. Chem.*, 2017, **89**, 6392-6398.

[6]   W. Liu, H. Dong, L. Zhang, Y. Tian, *Angew. Chem. Int. Edit.*, 2017, **56**, 16328-16332.

[7]   L. Zhang, Y. Han, F. Zhao, G. Shi, Y. Tian, *Anal. Chem.*, 2015, **87**, 2931-2936.

[8]   Q. Shen, X. Zhao, S. Zhou, W. Hou, J.-J. Zhu, *J. Phys. Chem. C*, 2011, **115**, 17958-17964.

[9]   J. M. Bray, A. J. Davenport, K. S. Ryder, M. M. Britton, *Angew. Chem. Int. Edit.*, 2016, **55**, 9394-9397.

[10] S. Wang, C. Liu, G. Li, Y. Sheng, Y. Sun, H. Rui, J. Zhang, J. Xu, D. Jiang, *ACS Sensors* 2017, **2**, 364-370.

[11] C. Ge, Q. Luo, D. Wang, S. Zhao, X. Liang, L. Yu, X. Xing, L. Zeng, *Anal. Chem.*, 2014, **86**, 6387-6392.

[12] Y.-J. Tong, L.-D. Yu, L.-L. Wu, S.-P. Cao, Y.-L. Guo, R.-P. Liang, J.-D. Qiu, *ACS Sustain. Chem. Eng.*, 2018, **6**, 9333-9341.

[13] D. E. Kang, C. S. Lim, J. Y. Kim, E. S. Kim, H. J. Chun, B. R. Cho, *Anal. Chem.*, 2014, **86**, 5353-5359.

[14] C. Lei, Z. Wang, Z. Nie, H. Deng, H. Hu, Y. Huang, S. Yao, *Anal. Chem.*, 2015, **87**, 1974-1980.

[15] Z. Yuan, N. Cai, Y. Du, Y. He, E. S. Yeung, *Anal. Chem.*, 2014, **86**, 419-426.

[16] X. Fang, Y. Liu, L. Jimenez, Y. Duan, G. B. Adkins, L. Qiao, B. Liu, W. Zhong, *Anal. Chem.*, 2017, **89**, 11758-11764.

[17] Y. Lin, C. Wang, L. Li, H. Wang, K. Liu, K. Wang, B. Li, *ACS Appl. Mater. Inter.*, 2015, **7**, 27262-27270.

[18] J. Hao, F. Liu, N. Liu, M. Zeng, Y. Song, L. Wang, *Sens. Actuators, B*, 2017, **245**, 641-647.

[19] Y. Ma, G. Xu, F. Wei, Y. Cen, Y. Ma, Y. Song, X. Xu, M. Shi, S. Muhammad, Q. Hu, *J. Mater. Chem. C*, 2017, **5**, 8566-8571.

[20] aB. Zhao, L. Zhou, L. Ma, Y. He, J. Gao, D. Li, Y. Jiang, *Int. J. Biol. Macromol.*, 2018, **107**, 2034-2043.

[21] bP. Wu, Y. He, H.-F. Wang, X.-P. Yan, *Anal. Chem.*, 2010, **82**, 1427-1433.